

Review

A Comprehensive Review on Development and Applications of Cross-Flow Wind Turbines

Zahra Sefidgar ¹, Amir Ahmadi Joneidi ^{2,3} and Ahmad Arabkoohsar ^{4,*}¹ Department of Mechanical Engineering, K. N. Toosi University of Technology, Tehran 19697-64499, Iran² Department of Mechanical Engineering, Amirkabir University of Technology (Tehran Polytechnic), Tehran 15916-34311, Iran³ New Technologies Research Center, Amirkabir University of Technology (Tehran Polytechnic), Tehran 15916-34311, Iran⁴ Department of Civil and Mechanical Engineering, Technical University of Denmark, 2800 Lyngby, Denmark

* Correspondence: ahmar@dtu.dk

Abstract: The rapid globalization of the energy crisis and the adverse effects of global warming have caused the need for non-conventional energy resources to be felt more than ever. As a result of this, vertical axis wind turbines (VAWT) have received much attention over the recent decades, and have thus been more developed and used worldwide. The cross-flow wind turbine (CFWT) is a wind turbine in the category of VAWTs, and perfectly suitable for urban applications due to its simplicity, high starting torque at low wind speed, and self-starting capability, even though its low power coefficient as its main drawback has slowed down its widespread use so far. The main aim of this paper is to review the scientific literature and recent developments in the field of CFWTs. The governing equations and turbulence models for the simulation of the turbine are discussed and various wind resource assessment methods for estimating potential site locations, different aspects, and wind energy harvesting systems from buildings are debated. The research gaps, challenges, and future possible works on such turbines and their applications are discussed. Investigations indicate that changing the rotor geometric parameters and adding innovative augmentation devices have been the most widely addressed approaches for making performance enhancement of the wind turbine in the literature. The critical performance-affecting parameters are improved by various innovative designs of the turbine structure or blades, as well as several augmentation techniques, such as guide nozzle, casing, windshield, guide vane, deflector, cowling, etc.

Keywords: cross-flow wind turbine; Banki wind turbine; power coefficient; RANS; building-scale wind turbines; urban wind energy



check for updates

Citation: Sefidgar, Z.; Ahmadi Joneidi, A.; Arabkoohsar, A. A Comprehensive Review on Development and Applications of Cross-Flow Wind Turbines.

Sustainability **2023**, *15*, 4679. <https://doi.org/10.3390/su15054679>

Academic Editor: Byungik Chang

Received: 30 November 2022

Revised: 27 January 2023

Accepted: 7 February 2023

Published: 6 March 2023



Copyright: © 2023 by the authors. Licensee MDPI, Basel, Switzerland. This article is an open access article distributed under the terms and conditions of the Creative Commons Attribution (CC BY) license (<https://creativecommons.org/licenses/by/4.0/>).

1. Introduction

1.1. Opening

For decades, the electric power supply has relied heavily on fossil fuels. Environmental pollution, limited sources of these fuels, and increasing energy demand have caused human concerns [1,2]. According to the predictions, fossil fuels will no longer be able to meet the growing energy demand. Due to the limited fossil fuel resources, their cost will also increase. Constant consumption of this type of energy will lead to an increase in environmental pollutants [3,4]; for example, three billion people still use polluting fuels and technologies for cooking, which leads to carbon dioxide production in their home environment [5]. In addition, the growing body of evidence shows this pollution directly correlates with adverse pregnancy outcomes and tuberculosis, with 3.8 million deaths annually [6–8]. Hence, the international community has recognized a comprehensive assessment of the user experience, health effects, and barriers to adopting improved energy to better energy sources [9]. Renewable energies can be a reliable solution to these problems [10], which are widely applicable in three main fields of thermal, transportation,

and electricity generation, especially in remote areas, and are constantly expanding [11,12]. There are various renewable energy resources, e.g., hydropower, marine, bio, solar, wind energy, etc. [13]. Wind energy is distinguished as one of the most cost-effective ways of electricity generation from renewable sources, and with high accessibility [14]. Wind energy is, today, the fastest-growing energy technology among all [15–19], leading to a significant jump in the global wind power capacity every year (see Figure 1).

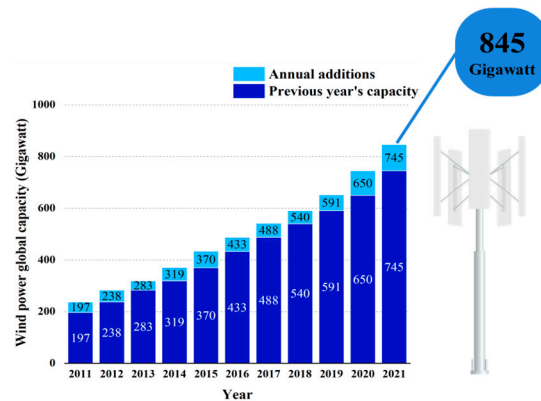


Figure 1. Wind power global capacity and annual additions, 2011–2021.

Wind energy can be captured by using wind turbines (WT), which are divided into two main categories based on the turbine's rotational axis: VAWT and horizontal axis wind turbine (HAWT) [14]. HAWTs with lift-type rotors perform better than VAWTs in terms of torque and power. The drag-type rotors of VAWTs produce lower performance values, but they are cost-effective, easy to start, and operate at lower wind speeds [20–23]. In the past, the most common type of turbine was large-scale HAWTs in wind farms [24]. However, in recent years, many studies have been conducted with the aim of harvesting wind energy from urban and semi-urban areas, showing that VAWTs perform better than HAWTs [25,26]. In fact, due to the wind characteristics in the urban environment and the advantages of VAWTs, such as low cost, noise and vibration, insensitivity to wind direction, visual impact, and public safety, these turbines are more attractive in urban and semi-urban areas [27,28]. One type of VAWT is the CFWT, which is very similar to the Savonius turbine geometrically [29]. The maximum theoretical efficiency of CFWTs is around 12–15% [30], while the efficiency of the Darrieus turbine, another type of VAWT, is about 35%. HAWTs' maximum efficiency could be as high as 45% [31].

1.2. Motivation and Article Structure

As shown in Table 1, many papers have already reviewed different types of VAWTs, except for CFWTs. The main reason behind this could be the low efficiency of CFWTs, depriving them of the central attention of research works as a promising energy technology. However, researchers have recently become more aware of the positive side of CFWTs, such as their high starting torque at low wind speed, low noise, being environmentally friendly, simplicity, reliability, and low costs, which make them suitable for small applications in areas with low wind speed, e.g., urban areas [32]. That is why many experimental and simulation studies have been done on them in recent years to make them more efficient and feasible. Therefore, there must be a review article presenting the latest findings and advances in this field and the further remaining gaps.

Table 1. Review papers in the field of VAWT.

Author	Year	Highlight
Tjiu et al. [33]	2015	Assessment of Darrieus configurations, including the drawbacks of each variation that kept them from being developed into large-scale rotors.
Alom and Saha [29]	2019	A comprehensive and systematic review of Savonius rotor blade profiles and shapes.
Tasneem et al. [34]	2020	Description of the state of urban wind farm technology and its different aspects.
Rajpar et al. [35]	2021	Development in the design and optimization techniques of wind deflectors for VAWTs.
Dewan et al. [36]	2021	Effect of various performance-influencing parameters and advances in the power augmentation techniques used for S-type Savonius rotors.
Karmakar and Chattopadhyay [37]	2022	A review of augmentation methods to increase the performance of VAWTs.
Cuevas-Carvajal et al. [38]	2022	Evaluating the effect of geometrical parameters on the performance of Savonius.

The main purpose of this paper is to categorize different methods for designing and improving the performance of CFWTs. For this, two approaches have been used: first, changing the rotor's geometric characteristics, and second, designing and adding the augmentation devices. Moreover, this article describes the applications, aspects, and challenges of CFWTs in urban and non-urban environments. The paper will pave the way for future research by answering the following questions:

- What was the history and evolution of the cross-flow rotor (CFR)?
- What are the features and applications of CFWTs?
- What are the performance improvement methods and common modeling strategies?
- What features and aspects make CFWTs attractive for harvesting energy in urban environments?
- What is the necessity to find a suitable site location?

1.3. Research Methodology and Analysis

A systematic literature search consisting of three steps, depicted in Figure 2, was applied to create a database of relevant publications. In the first step, the initial search was performed with two main keywords throughout the text on four search platforms. Search engines are unable to distinguish terms such as “crossflow”, “cross flow”, and “cross-flow”. Therefore, all terms were added to the query string with the logical operators (AND and OR). Many results from the searching step were irrelevant; thus, items such as datasets, reports, patents, books, book chapters, and policy documents were filtered in the second step.

Additionally, duplicate articles were removed and the initial keywords were considered for searching in the title, abstract, and keywords. Search results with different keywords and domains in three platforms can be seen in Table 2. In the last step, the text of the articles needed to be examined more thoroughly to be logically compatible with the purpose of this review paper. The backward, forward, and author citation searches were used to find articles with different keywords to reach the final database.

It should be noted that the analysis of the gathered publications was done in the bibliometric analysis step. Its purpose was to use keywords co-occurrence evaluation to identify relevant secondary keywords. This evaluation was done with VOSviewer, a text mining software for constructing and visualizing bibliometric networks. All words in the title, abstract, and keywords in the gathered publications were extracted from Scopus and Web of Science and were filtered by considering a minimum of three occurrences based on co-occurrence analyses. Figure 3 illustrates the network visualization of the co-occurrence map of the keywords. 111 and 183 articles were evaluated in Figure 3a,b, respectively. The size of the circles is based on the weight of the word repetition during the article evaluation process. The lines indicate the relationship between the two terms used in an article, and different colors indicate clustering (thematic classification). As can be seen, the words

WT, VAWT, performance, and C_p were the most frequent and were considered secondary keywords.

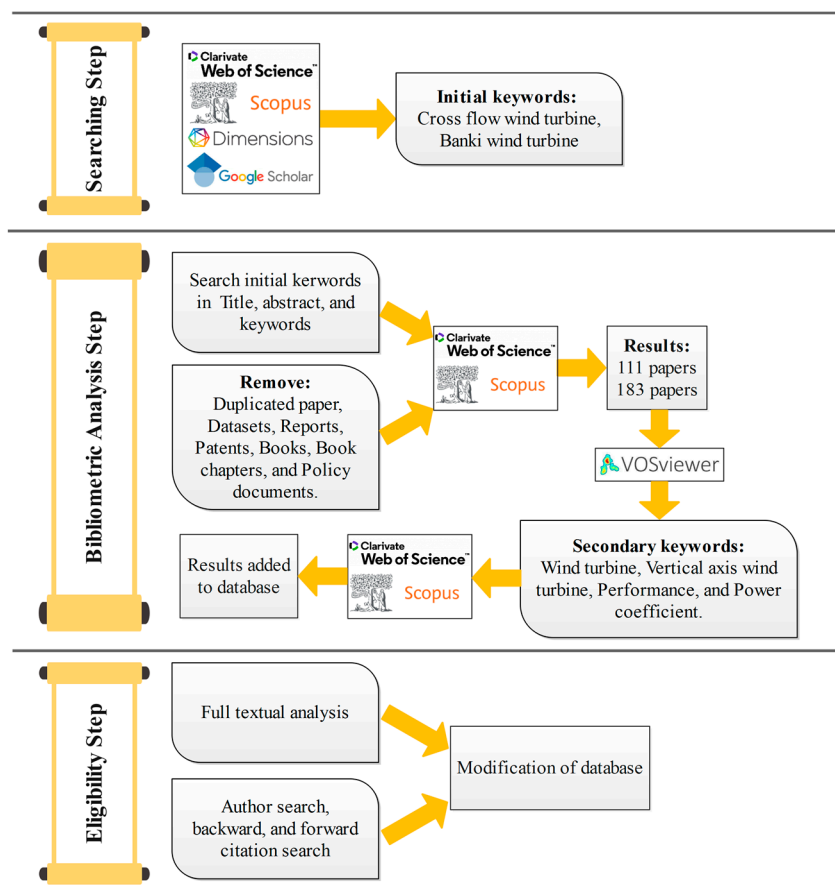


Figure 2. Literature search methodology.

Table 2. Search results in three platforms based on initial and secondary keywords (Topic = title, abstract, keywords) (The starred results will be used in the publications’ trend analysis).

No	Keywords	Search Domain	Web of Science	Scopus	Dimensions
1	“Cross-flow wind turbine”	All field Topic	14 14	170 37	282 70
2	(“Cross-flow” OR “Cross flow” OR “Crossflow” OR “Banki”) AND “wind turbine”	All field Topic	115 111 *	2425 183 *	6612 169 *
3	(“(“Cross-flow” OR “Cross flow” OR “Crossflow” OR “Banki”)) AND “wind turbine”) AND “Vertical axis”	All field Topic	46 46	1027 66	2644 45
4	(“(“Cross-flow” OR “Cross flow” OR “Crossflow” OR “Banki”) AND “wind turbine”) AND “Vertical axis” AND “power coefficient” AND “performance”	All field Topic	14 14	291 16	1164 17

There is an analysis to determine the historical development and trends of publications related to this field (the second row with * in Table 2). Figure 4 illustrates the number of publications based on every five-year period from 1998 to 2022 on the three platforms. This figure indicates that the number of publications has continuously increased, and more than 60% of the papers have been published only in the last ten years. This analysis finds the

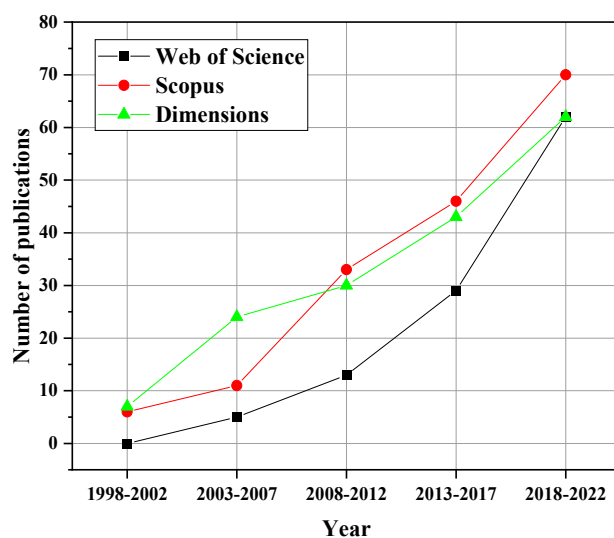


Figure 4. The number of publications on a 5-year basis.

2. WTs and Principles

2.1. Classification of WTs

WTs could be classified from different perspectives. As Figure 5 demonstrates, the classification could be based on the method of turbine action (aerodynamic force), the location where the turbine is placed, the way the speed of the turbine is managed, and last but not least, the configuration of the turbine about the axis of rotation. Regarding how the aerodynamic force acts on the turbine, one could say that WTs may be designed to act based on the drag force, lift force, or a combination of these two from the airflow. Ancient windmills were mainly built based on drag force action, while modern large-scale WTs rely on a very high lift force rather than a drag force (a high lift-to-drag ratio, up to 200). WTs can be erected either onshore or offshore; where for the latter the higher wind power over open waters (oceans) with a higher energy density could be taken advantage of. Constant speed WTs always rotate at the same generator/rotor speed, regardless of the wind speed changes. Thus, the tip speed ratio (TSR) changes, and the WT will have optimal aerodynamic performance only at a particular wind speed. Variable speed WTs allow the generator/rotor speed to change proportionally to the wind speed between the cut-in and rated speed. As a result, the TSR and the performance remain at an optimum point [39].

For the latter point, WTs could be either VAWTs, HAWTs, cross-axis wind turbines (CAWT), or bladeless. VAWTs and HAWTs have a vertical and horizontal blade rotation axis, respectively. However, a new experimental cross-linked turbine called CAWT is made by combining these two types of blades (three vertical and six horizontal), allowing to capture wind energy from both vertical and horizontal directions [40,41]. The bladeless turbines, which generate electricity by vibrating mechanisms, are still under development and are a little bit unknown. Notwithstanding they have low power efficiency, they are cost-efficient [42]. Some turbines do not fit into the above categories; for instance, INVELOX, IMPLUX, Cooling tower updraft, and Kite that do not have a rotating axis, and O-Wing that has a variable rotating axis.

Two well-known types of VAWTs are Darrieus and Savonius [43,44]. Figure 6 shows different types of Darrieus. For the first time in 1926, Georges Darrieus invented his turbine designs (Phi-rotor and Giromill) [45], which rotate by the lift force generated in the blades [46] and have a theoretical efficiency of about 40% [31]. The Savonius was invented by Sigurd Savonius in 1929 [47] and consists of at least two half-cylinders. As shown in Figure 7, the drag force in the concave part of the blades is more than the one in the convex part, which causes the turbine to rotate around its axis. $C_{p,max}$ in Savonius is only around 15% [30]; thus, its efficiency is lower than Darrieus, but it has a good starting torque at low wind speed [32].

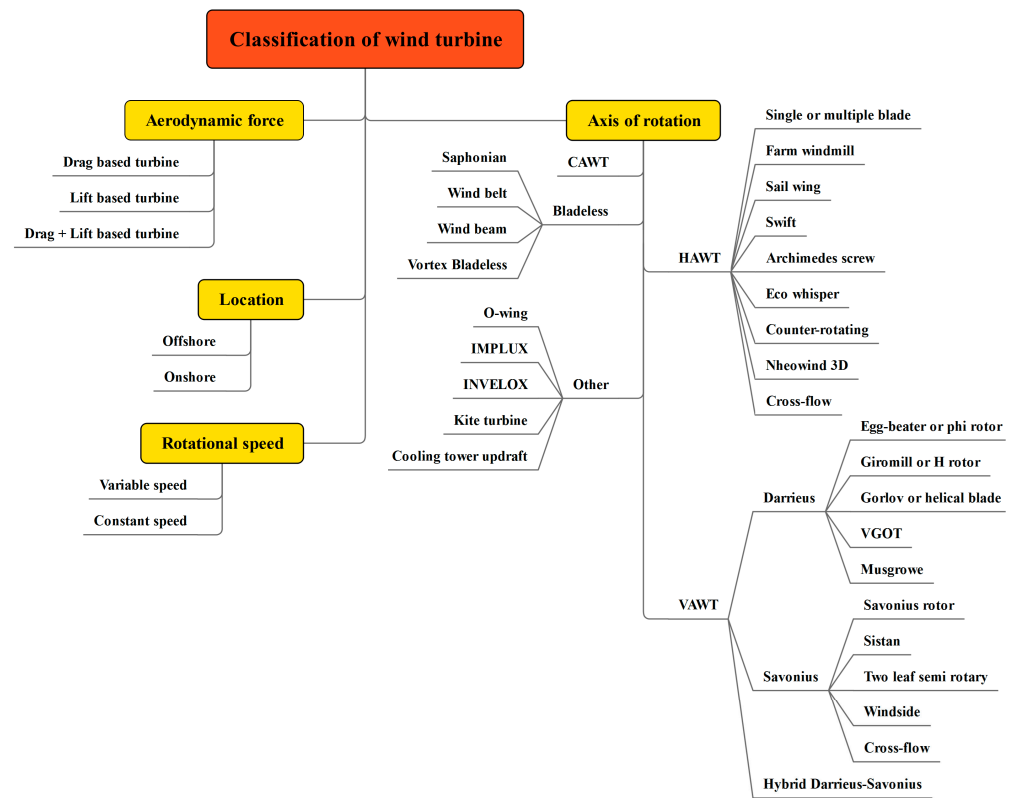


Figure 5. Classification of WTs from different angles.

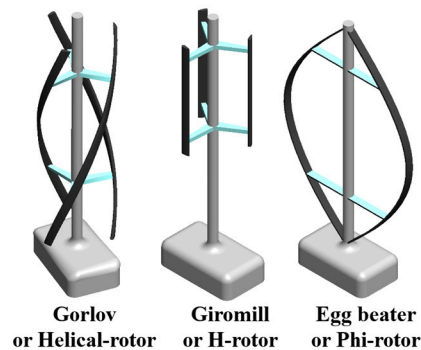


Figure 6. Different types of Darrieus turbines.

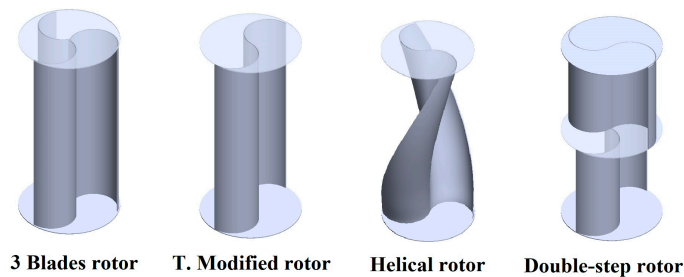


Figure 7. Different types of Savonius turbine blades.

One of the sub-branches of Savonius is the CFWT, which is geometrically similar [29]. Also, CFWTs can be installed and operated on two vertical and horizontal axis modes, so they are classified as HAWTs and VAWTs. Small-scale wind turbines (SSWTs) have a capacity of up to 16 kW and rotor diameter between 0.5 to 10 m [48]. A CFWT with

500 watts nominal power capacity produces 3.2 MWh/year at a maximum wind speed of 11.5 m/s [49–51]; therefore, CFWTs can be counted as an SSWT.

2.2. Governing Equations and Turbulence Models

The governing equations are given by the Incompressible Navier-Stokes equation for rotating objects (relative velocity), including the conservation of mass and momentum equations, as given in Equations (1) and (2).

$$\frac{\partial \rho}{\partial t} + \nabla \cdot \rho \vec{u}_r = 0 \quad (1)$$

$$\frac{\partial}{\partial t} (\rho \vec{u}_r) + \nabla \cdot (\rho \vec{u}_r \vec{u}_r) + \rho (2\vec{\omega} \times \vec{u}_r + \vec{\omega} \times \vec{\omega} \times \vec{r}) = -\nabla p + \nabla \tau_r + \vec{F} \quad (2)$$

In Equation (2), two acceleration terms represent rotation. These terms include the Coriolis acceleration and the centripetal acceleration, which are defined by $2\vec{\omega} \times \vec{u}_r$ and $\vec{\omega} \times \vec{\omega} \times \vec{r}$ respectively. In these equations, \vec{u}_r is the relative velocity, $\vec{\omega}$ is the angular velocity of the rotor domain, \vec{r} is the radial position from the origin of the rotating domain, p is the static pressure, τ is the stress tensor, and \vec{F} refers to external body forces. τ is given by:

$$\tau = \mu \left[\left(\nabla \vec{u}_r + \nabla \vec{u}_r^T \right) - \frac{2}{3} \nabla \cdot \vec{u}_r I \right] \quad (3)$$

I , the unit tensor, refers to the effect of volume dilation.

According to the approximations required to solve the turbulent stress equations, various turbulence models have been developed in the past. Each model offers different advantages according to the operating conditions for which it has been developed [52]. However, the simplest complete turbulence models for rotating airfoil problems are realizable k - ε and k - ω SST. Both models introduce two transport equations: first, the turbulence kinetic energy (k), and second, specific dissipation rate (ω) in the k - ω SST model or dissipation rate (ε) in the realizable k - ε model.

The realizable k - ε is a semi-empirical two-equation turbulence model that significantly differs from the standard k - ε model proposed by Launder and Spalding [53] in two respects: realizable k - ε contains a different eddy-viscosity formulation and employs a modified transport equation to express the dissipation rate. It means that the eddy-viscosity coefficient (C_μ) is a function of local flow parameters; nonetheless, it is constant in the standard k - ε model. The realizable k - ε has become increasingly popular in the CFD community due to its reasonable accuracy, improved performance, and economy. It is recommended for rotating objects and free shear layer flows [54].

The transport equations for k and ε are:

$$\frac{D\rho k}{Dt} = \frac{\partial}{\partial x_j} \left[\left(\mu + \frac{\mu_t}{\sigma_k} \right) \frac{\partial k}{\partial x_j} \right] + G_k + G_b - \rho\varepsilon - Y_M + S_k \quad (4)$$

$$\frac{D\rho\varepsilon}{Dt} = \frac{\partial}{\partial x_j} \left[\left(\mu + \frac{\mu_t}{\sigma_\varepsilon} \right) \frac{\partial \varepsilon}{\partial x_j} \right] + \rho C_1 S \varepsilon - \rho C_2 \frac{\varepsilon^2}{k + \sqrt{v\varepsilon}} + C_{1\varepsilon} \frac{\varepsilon}{k} C_{3\varepsilon} G_b + S_\varepsilon \quad (5)$$

where,

$$C_1 = \max \left[0.43, \frac{n}{n+5} \right] \quad (6)$$

$$n = S \frac{k}{\varepsilon} \quad (7)$$

$$S = \sqrt{2S_{ij}S_{ij}} \quad (8)$$

In these equations, G_k and G_b are the turbulence kinetic energy generation due to the mean velocity gradients and buoyancy, respectively. Likewise, they are calculated similarly to the standard k- ε model. Y_M is the contribution of the fluctuating dilatation in compressible turbulence to the overall dissipation rate, M_t is the turbulent Mach number, μ_t is the turbulent dynamics viscosity, S_k and S_ε are user-defined source terms, and σ_ε and σ_k are the turbulent Prandtl numbers for ε and k , respectively. Other parameters are:

$$Y_M = 2\rho\varepsilon M_t^2 \quad (9)$$

$$\mu_t = \rho C_\mu \frac{k^2}{\varepsilon} \quad (10)$$

$$C_\mu = \frac{1}{A_0 + A_s \frac{kU^*}{\varepsilon}} \quad (11)$$

$$U^* = \sqrt{S_{ij}S_{ij} + \tilde{\Omega}_{ij}\tilde{\Omega}_{ij}} \quad (12)$$

$$\tilde{\Omega}_{ij} = \Omega_{ij} - 2\varepsilon_{ijk}\omega_k \quad (13)$$

$$\Omega_{ij} = \overline{\Omega_{ij}} - \varepsilon_{ijk}\omega_k \quad (14)$$

$$A_s = \sqrt{6}\cos\phi \quad (15)$$

$$\phi = \frac{1}{3}\cos^{-1}\left(\sqrt{6}W\right) \quad (16)$$

$$W = \frac{S_{ij}S_{jk}S_{ki}}{\tilde{S}^3} \quad (17)$$

$$\tilde{S} = \sqrt{S_{ij}S_{ij}} \quad (18)$$

$$S_{ij} = \frac{1}{2}\left(\frac{\partial u_j}{\partial x_i} + \frac{\partial u_i}{\partial x_j}\right) \quad (19)$$

The constants values are: $A_0 = 4.04$, $C_{1\varepsilon} = 1.44$, $C_2 = 1.9$, $\sigma_k = 1.0$, and $\sigma_\varepsilon = 1.2$.

The standard k- ω model is based on the Wilcox k- ω model [55], which predicts free shear flow spreading rates and agrees with measurements for far wakes, mixing layers, and radial, plane, and round jets. Nevertheless, it is very sensitive to free flow. The k- ω SST model, which was developed by Menter [56,57], is a combination of the k- ω model in near-wall regions and the k- ε model outside the boundary layer. In other words, the k- ω SST model only benefits from the k- ω and the k- ε models. These features make the k- ω SST model more reliable and accurate than a standard k- ω model for wider types of flow (e.g., low-pressure gradient flows, airfoils, and ultrasonic shock waves). The k- ω SST mode equations are expressed as:

$$\frac{D\rho k}{Dt} = \tau_{ij}\frac{\partial u_i}{\partial x_j} + \beta^*\rho\omega k + \frac{\partial}{\partial x_j}\left[(\mu + \sigma_k\mu_t)\frac{\partial k}{\partial x_j}\right] \quad (20)$$

$$\frac{D\rho\omega}{Dt} = \frac{\gamma}{v_t}\tau_{ij}\frac{\partial u_i}{\partial x_j} - \beta\rho\omega^2 + \frac{\partial}{\partial x_j}\left[(\mu + \omega_k\mu_t)\frac{\partial \omega}{\partial x_j}\right] + 2\rho(1 - F_1)\frac{1}{\omega}\frac{\partial k}{\partial x_j}\frac{\partial \omega}{\partial x_j} \quad (21)$$

The auxiliary relations are written as below:

$$\beta^* = \frac{\varepsilon}{k\omega} \quad (22)$$

$$\tau_{ij} = -\rho\overline{u'_i u'_j} = \mu_t\left(\frac{\partial u_i}{\partial x_j} + \frac{\partial u_j}{\partial x_i} - \frac{2}{3}\frac{\partial u_k}{\partial x_k}\delta_{ij}\right) - \frac{2}{3}\rho k\delta_{ij} \quad (23)$$

$$v_t = \frac{a_1 k}{\max(a_1 \omega, \Omega F_2)} \quad (24)$$

$$F_1 = \tanh \left\{ \left[\min \left[\max \left(\frac{\sqrt{k}}{0.09 \omega y}, \frac{500 v}{y^2 \omega} \right), \frac{4 \rho \sigma_{\omega 2} k}{C D_{k \omega} y^2} \right] \right]^4 \right\} \quad (25)$$

$$F_2 = \tanh \left\{ \left[\max \left(\frac{2 \sqrt{k}}{0.09 \omega y}, \frac{500 v}{y^2 \omega} \right) \right]^2 \right\} \quad (26)$$

$$C D_{k \omega} = \max \left(2 \rho \sigma_{\omega 2} \frac{1}{\omega} \frac{\partial k}{\partial x_j} \frac{\partial \omega}{\partial x_j}, 10^{-20} \right) \quad (27)$$

$$\phi = F_1 \phi_1 + (1 - F_1) \phi_2 \quad (28)$$

The empirical constants of the k - ω SST model are: $\beta^* = 0.09$, $\beta_1 = 0.075$, $\beta_2 = 0.0828$, $\gamma_1 = 0.5532$, $\gamma_2 = 0.4404$, $\sigma_{k1} = 0.85$, $\sigma_{k2} = 1.0$, $\sigma_{\omega 1} = 0.5$, $\sigma_{\omega 2} = 0.856$, and $a_1 = 0.31$.

Specific tip speed ratio (TSR or λ) measures the linear velocity of the blade tip (U) against the wind speed (V). It is given as [58]:

$$\lambda = \frac{U}{V} = \frac{\tilde{\omega} R_r}{V} = \frac{\pi N D}{60 V} \quad (29)$$

N is the rotational speed. The relationship between total wind power (P_W) and wind speed (V) is:

$$P_W = \frac{1}{2} \rho_{air} A_r V^3 \quad (30)$$

$$A_r = 2 R_r H_r \quad (31)$$

In WTs, the wind hits the blades and rotates them around the turbine axis. As a result, the generator connected to this axis generates AC power. The general relationship between wind power and turbine power is established by a factor called C_P , a variable parameter with wind direction (α), and TSR. Theoretically, the maximum C_P can be up to the Betz limit of 59.3% [59]. This relationship is shown in Equation (32), and the C_T is calculated according to Equation (33) [60].

$$P_t = P_W C_P(\lambda, \alpha) = \frac{1}{2} C_P(\lambda, \alpha) \rho_{air} A_r V^3 \quad (32)$$

$$C_T = \frac{T}{\frac{1}{2} \rho_{air} A_r V^3} \quad (33)$$

The C_P and C_T are the main parameters that define the turbine performance related to the TSR.

$$C_T = \frac{C_P}{\lambda} \quad (34)$$

According to Equation (35), the aspect ratio is defined as the ratio of rotor height to rotor diameter [61].

$$\text{Aspect Ratio} = \frac{H_r}{D_r} \quad (35)$$

Other parameters in this field include the angle of attack, cut-in speed, and cut-off speed. The angle of attack defines as the angle between the chord line and the wind velocity vector [62]. Cut-in speed is the minimum wind speed at which the turbine starts to spin. Similarly, cut-off speed is the maximum wind speed that the turbine operates at. If the wind speed exceeds this limit, the turbine blades will stop, and no power will be generated to prevent damage or failure [61].

3. CFWTs

3.1. History of CFR

A CFR is used in fans, hydro turbines, and WTs. The first written and recorded type of CFR can be traced back to a particular invention, the Cross-Flow Fan (CFF), in 1891 by Paul Mortier with patent number 215,662 in France. Then, it was registered in the United States [61] by correspondence. The main purpose was to utilize mine ventilation. Still, for two decades, the CFF was overlooked, took enough attention, and was left under the shadow beneath the development of axial flow fans.

There was a re-emergence of interest in the late 1920s and early 1930s, with a variety of industrial inventions in different applications such as drying grain [63], air conditioning [64,65], and injecting pulverized fuel into furnaces [66,67]. Nevertheless, the main advancement of CFF design began with detailed studies into their behavior in the late 1930s. Currently, CFFs are widely used in air conditioners, air curtains, household heaters, automotive air conditioning, ventilation, vertical take-off and landing aircraft, unmanned aerial vehicles, and underwater fan-wing vehicles due to their large capacity of mass flow and size compactness.

Meanwhile, Anthony Michell designed the Cross-Flow Hydro Turbine (CFHT) in 1903, and Donat Banki found his theoretical approach, which later registered his idea in 1922 [68]. At the same time, Fritz Ossberger developed Michell's design and patented it [69], [70]. Therefore, CFHT generally has been recognized as the Banki-Michell turbine or the Ossberger turbine. Several studies have been performed to optimize and enhance the CFHT efficiency and most application of the CFHT is used in hydropower plants.

In the early 21st century, several researchers [71–73] suggested that CFR could be used to absorb wind energy as a CFWT. However, about two decades earlier, Japanese researchers [74–80] made great efforts to determine the fluid flow characteristics around a CFWT. The growing demand for electricity and the benefits and applications of CFWTs led to much research in recent years to develop and improve their efficiency, C_p , and C_T .

3.2. Working Principle and Applications of CFWT

As shown in Figure 8, the CFWT is typically made of 6 to 24 blades and cylindrical shapes in single or multi-stages. This number of blades depends on the rotor diameter ratio, efficiency, cut-in, and cut-off. This figure shows components of CFWTs, such as the rotor, deflector, stand, and case. The deflector, which conducts the airflow into the rotor blades to increase the turbine's efficiency, is an optional augmentation device [81]. In addition, it is made in different shapes, sizes, and angles. A case holds all components together and is fixed to the ground or foundation by a stand. A power regulation system is required to adjust the output power in changing wind speeds or to prevent damage to the turbine and generator when the wind speed exceeds the cut-off speed. The controller unit finds the critical conditions by various sensors; thereby, it activates the braking system [82]. The methods for the brake are mechanical, electromagnetic, or mechanical-electromagnetic braking [83].

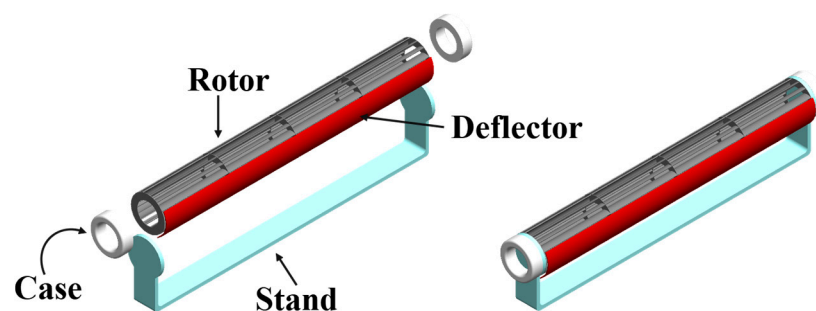


Figure 8. The structure and components of a CFWT.

Figure 9 depicts two ways to install a CFWT: standing (VAWT) and sitting (HAWT). Turbine installation methods are determined based on available space and the installation site specifications [49]. Buildings with vaulted and rounded roofs are the optimum roof shape for installation [84,85].

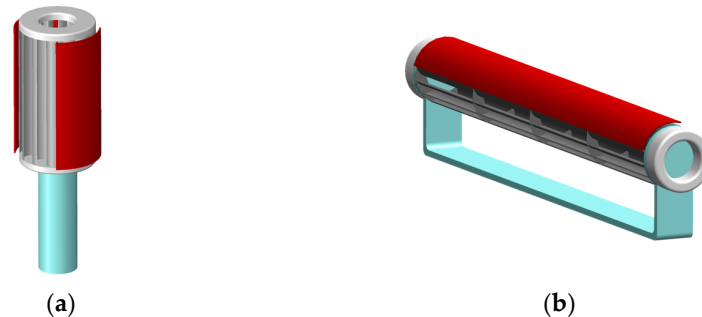


Figure 9. CFWT is mounted on the roof of the house in installation mode (a) VAWT and (b) HAWT.

The main application of CFWTs is to generate electricity from the airflow. This flow is created by the movement of vehicles on busy highways. The clean energy can be generated by installing many turbines in median strips [86–92] and using generated electricity on highway lights, traffic lights, traffic control cameras, pedestrian lights, and power supplies for electric vehicle charging stations. Additionally, the turbine can be installed on the runway, which uses the airflow, which is created by the movement of the aircraft, to produce energy [93]. CFWTs can also be used as a wave energy converter in Oscillating Water Columns (OWC), which utilizes the air's kinetic energy caused by ocean waves [94–96].

3.3. Advantages and Disadvantages of CFWTs

The CFWT has a high C_T at low wind speed. Therefore, it is an excellent candidate to use as a self-starting turbine. Low noise, remarkable stability, and a cut-in speed lower than 2 m/s make CFWTs suitable for urban areas. Moreover, its simple structure needs low maintenance costs and is not as dangerous for flying birds as HAWTs. Depending on the size and structure of the site, different methods can be used for installation. In addition, due to the low starting speed, it can be installed near the ground (0.5 m to 10 m above the ground) [48].

According to Figure 10, the $C_{P,max}$ of this turbine (0.12) is very low compared to the others. Nevertheless, by using augmentation devices, its C_P can be increased. Since the CFWT is one of the SSWTs, it cannot generate energy at high wind speeds (approximately more than 20 m/s). CFWT material is cheaper, lighter in weight, and possesses higher strength than industrial turbine material [97]. Therefore, the blade rotation is expected to be stopped in the high-speed range to prevent damage to the turbine components [48,98].

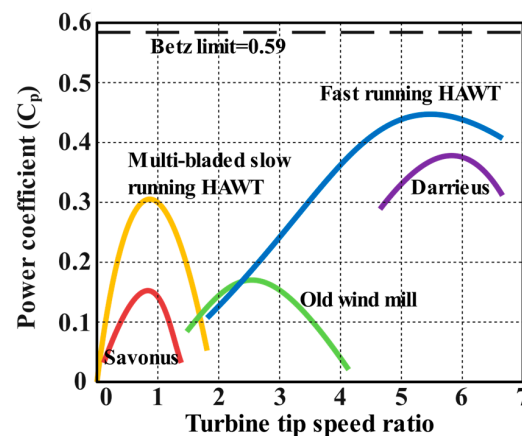


Figure 10. The C_P - λ diagram for WTs.

4. Parameters Affecting the Performance of CFWT

The aerodynamic performance prediction of the CFWT discussed in the previous section is crucial to its design optimization. For the performance analysis, different parameters, such as C_T , C_p , and aerodynamic loads, must be determined, and the rotor's flow field must be visualized. Over the last two decades, computational and experimental techniques for fluid flow analysis around the blades have significantly developed.

Kawamura et al. [99,100] showed a 2D numerical method to calculate the complex flow fields around the cylindrical 12-bladed CFWT and computed the C_T and C_p . They used the Incompressible Navier-Stokes equation with a rotating coordinate system, which rotates at the same speed as the CFWT, and is used to simplify the boundary conditions on the blades. The fractional step method is used to solve these equations, and a third-order upwind scheme is chosen to approximate the non-linear terms. Also, the C_p has its maximum value, 0.11, around $\lambda = 0.28$, and C_T is inversely related to λ . Kono et al. [101] performed a wind tunnel experiment (WTE) at $\lambda = 0.4$ to measure the flow characteristics around a CFWT and CFD simulation at $\lambda = 0.1, 0.4, \text{ and } 0.7$. The CFD approach validated the WTE measurements and confirmed that with an increase in λ , the velocity deficit and the turbulence kinetic energy were generally increased on the leeward of the return side of the WT.

In contrast, they were generally decreased on the leeward of the drive side of the WT. In another WTE investigation at wind speeds from 4 to 10 m/s, Sivamani et al. [102] reported that the peak power coefficient, C_p , max of 0.0485, was obtained for TSR = 0.50. Using a CFWT with the eight blades arrangement, Al-Maaitech [103] reported a maximum C_p of 0.30 at λ between 0.35 to 0.60. The experimental and numerical studies for CFWTs involving alterations in the geometrical parameters, e.g., number of blades, rotor arrangement, blade orientation and shape, and the number of stages, are discussed. Similarly, the investigations regarding augmentation devices are also addressed in the subsequent section.

4.1. Number of Blades

Rotor blades number plays a key role in determining specific performance parameters at different wind speeds. Numerous studies have been made regarding the optimum rotor blade number. Their results indicate that this number can vary depending on various conditions, such as the direction of rotation, type of installation (VAWT or HAWT), blade shapes, wind velocity, and Reynolds number. In most studies, 12 [104–106] and 16 [107–109] blades were recommended that can lead to the highest performance. However, other studies determined that 7 [110], 18 [111], 20 [112,113], and 22 [114,115] blades were the best choices. Table 3 presents studies on the number of CFWT blades.

4.2. Configuration and Arrangement

Pertiwi et al. [116] focused on a WTE using linear configuration to know the effect on the turbine performance. The distance between two turbines to be 1.5D, 2D, and 2.5D (D represents the outer diameter of CFWT). The aspect ratio of each turbine is 1 (200 mm in diameter and 200 mm in height). They informed that when two CFWTs are arranged linear and parallel to the wind flow, the downstream turbine is shielded from the inlet flow by the upstream turbine. Therefore, the downstream turbine interferes with the turbulence and vortex formation region and wake dynamics of the upstream turbine. Also, their results show that the C_p increased with increasing the distance between two turbines. In other words, it reached the highest C_p at the 2.5D distance, 0.122 in the upstream turbine and 0.082 in the downstream turbine.

In a similar investigation, Arifin et al. [104] positioned two CFWTs in a linear configuration and adjusted them to rotate in opposite directions. They used a wind tunnel with a diffuser and a fan to control the flow velocity. Wind speed was measured at three spots: a, b, and c. Their study concluded that the CFWT linear with opposite rotation could improve the performance of WTs. Moreover, Sato et al. [117] developed a numerical method to calculate the flow fields around multiple CFWTs in a linear arrangement. They computed

the effect of numerous lined CFWTs and their dependency on the incoming wind direction at various boundary conditions to investigate how they interact.

In most cases, WTs are not installed linearly. Rather, they are installed in a farm arrangement. To better operation, a proper arrangement of WTs on the wind farm should be determined to decrease wake. For this purpose, Oktavitasari et al. [118] studied the wind farm in an aligned and staggered configuration with 2-dimensional numerical analysis using ANSYS Fluent CFD software. Figure 11 shows their configuration, in which the distance between the turbines was 0.5D, 1D, and 1.5D (D represents the outer diameter of the CFWT). Their study revealed that the best arrangement is a staggered configuration within the distance S1:S2 of 0.5D:0.5D. In this arrangement, the power density of the wind farm achieved the highest level of 1.641 W/m².

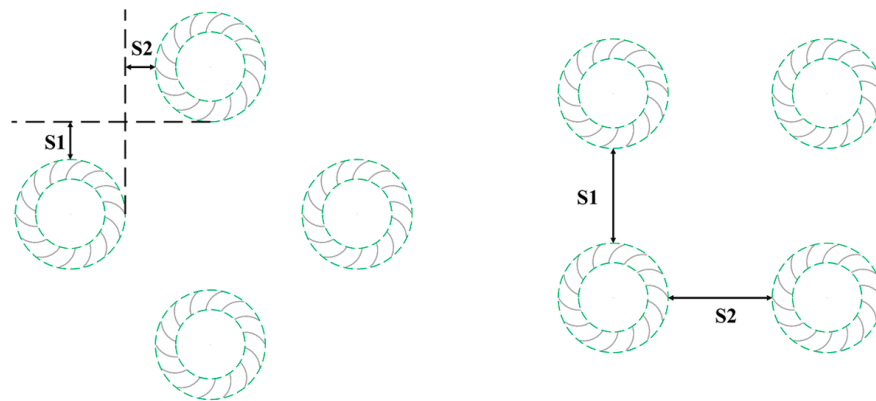


Figure 11. The configuration WT aligned and staggered of wind farm.

Other research studied the feasibility of using CFWTs as single rotors in VAWTs or as blades in HAWTs. Pujol et al. [115] numerically investigated the flow field characteristics, the drag-to-lift ratio, C_T , and C_P using the 2D-CFD method (ANSYS Fluent). Furthermore, they validated all cases with experimental data obtained in a WTE under runaway conditions. Their simulation showed that the CFWT in the HAWT needed an external (non-wind) power supply to rotate the CFWT at a constant rotational speed. The drag, lift, and torque coefficients in the whole rotors for a 2-D simulation show an oscillating behavior with a dominant frequency. The source of this dominant frequency is in the non-alternating vortex shedding, which is detected downstream of the rotor. Because of its amplitude, it must be considered to prevent resonances when designing the turbine structure. This effect is not clearly observed in VAWT mode. The $C_{P,max}$ in the VAWT is 0.19, which occurred at very low values of TSR (≈ 0.3). However, the available net power of the HAWT (extracted power minus required to rotate the rotors) is much lower, with a maximum net power coefficient $C_{P,net} = 0.14$ for TSR = 0.9 and $\alpha = 0.7$ (the cylinder spin ratio). Thus, it is necessary for HAWT applications to design the CFR with aerodynamic blades so that the lift-to-drag ratio is low and, simultaneously, has low resistant torques.

4.3. Number of Stages

The CFWT undergoes large fluctuations in torque at different azimuthal angles during its rotation. Such fluctuations in the turbine structure can significantly affect its useful life cycle and thus call its feasibility into question. Stacking single turbines on top of each other with distinct phase differences between the blades (phase shift angle) has been a well-known technique in WT optimization. Such an arrangement has led to an outstanding reduction in torque fluctuations. Several studies have reported better performance for multi-stage turbines than conventional single-stage designs. Due to the effectiveness of multi-stage turbines, Fahrudin et al. [119] conducted an experimental study to investigate the effect of multi-stage CFWTs on wind energy extraction. They have tested three types of rotors (single-stage, double-stage, and triple-stage) with different phase shift angles of

0° , 6° , and 12° in the wind tunnel at wind speeds of 3 to 4.85 m/s. Based on their results, $C_{P,max} = 0.13$ was obtained for double-stage and $C_{P,max} = 0.12$ for 12° phase shift angle at wind speed 4.05 m/s. They also mentioned that multi-stage and phase shift provide good value, reducing the negative torque.

4.4. Blade Orientation and Shape

The turbine angular rotation and the generated torque mainly dependent on drag force determine the CFWT power. Similarly, the drag force applying to the turbine relies on the blade profile and its alignment, which makes the blade shape an important aspect of the design. The conventional blades were semi-circular with an arc of 180° , and researchers provided blade modifications to increase the turbine performance over time. These modifications included rotor diameter [120,121], rotor diameter ratio [112,113], angle of blade [111,122,123], thickness [114], and blade circumferential length [110]. However, the aspect ratio is an important parameter; research has yet to be done on CFWTs.

Rotor diameter ratio means the ratio of the outer diameter to the inner diameter of the rotor blade. Experimental and CFD studies show that by choosing diameter ratios of 0.58, 0.63, 0.68, and 0.73, and furthermore, by keeping the outer diameter constant, the highest C_P of 0.049 [112] and 0.5 [113] were reported for a diameter ratio of 0.68. The discrepancy comes from working with different blade shapes, aspect ratios, Reynolds numbers, various simulation assumptions, and laboratory errors. In addition, the angle of blade (θ) (Figure 12a), which is the angle between the tangent line to the rotor circumference and the endpoint of the blade, is investigated. In a study [122] with angles of 30° , 45° , 60° , and 90° , the best result was obtained at 45° , with $C_P = 0.41$ at TSR = 0.76. Similarly, in another study [111] with angles of 45° , 60° , and 75° , the highest performance occurred at 45° , with $C_{P,max} = 0.45$ at TSR = 0.3. According to Figure 12b, Option-A, with an average torque of 3.2 Nm, performs higher than Option-B [123]. A 2D transient simulation [87] was performed with ANSYS Fluent on four thicknesses of blades of 2.6, 10, 15, and 20 mm to investigate the effect of blade thickness. The highest C_P was 0.5 at TSR = 0.2, obtained by a maximum blade thickness of 20 mm. The circumferential blade length study [110] showed that for six- and seven-blade turbines with 30° circumferential cuts at the front and back of the blade, the C_P increased from 0.043 for the conventional blades to 0.24 for a seven-blade turbine with double cut blades. A summary of the optimization studies discussed above is provided in Table 3.

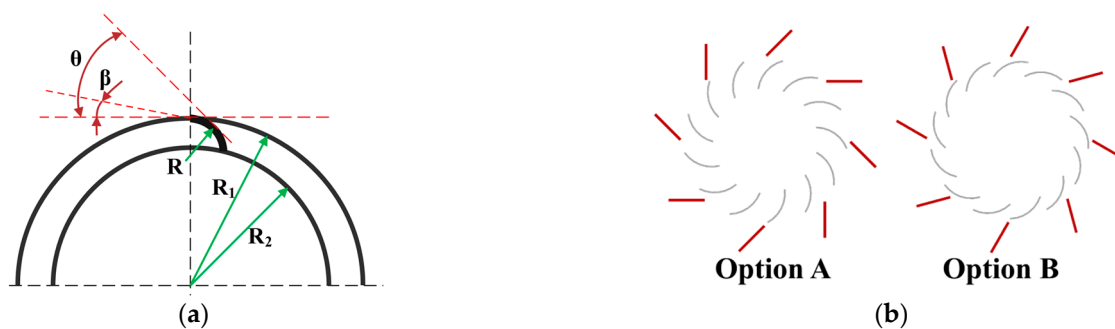


Figure 12. (a) The blade parameters of the turbine and (b) Design options of CFWT.

Table 3. Summary of the investigation conducted to determine the configuration and modify blade shape and number.

Author	Year	Method	Turbine Design	Optimum Value (s) of Parameter	Remarks	Maximum C_p	Maximum C_T
Arifin et al. [104]	2021	Experimental	Number of blades = 12, 16, and 20 Wind speed = 8 and 10 m/s Aspect Ratio = 1 The effect of opposite direction rotation and the linear configuration	Number of blades = 12 Wind speed = 10 m/s	Opposite rotation and the linear configuration increase performance	0.169 at TSR = 0.4	0.703
Pertiwi et al. [116]	2020	Experimental	Linear configuration Turbine distance = 1.5D, 2D, and 2.5D Aspect Ratio = 1 Wind speed = 5, 6, and 7 m/s	Wind speed = 7 m/s linear configuration 2.5D	$C_{p,max}$ is 0.122 on upstream turbine and 0.082 on downstream turbine	-	-
Hidayat and Ismail [111]	2019	CFD-2D	Number of blades = 18 and 20 Angle of blade = 45°, 60°, and 75° Aspect ratio diameter = 0.68 Wind speed = 2 to 5 m/s	Number of blades = 18 Angle of blade = 45°	-	0.45 at TSR = 0.3	3 at TSR = 0.1
Wikantyoso et al. [114]	2019	CFD-2D	Blade thickness = 2.6, 10, 15, and 20 mm Number of blades = 18, 20, and 22 TSR = 0.1 to 0.5	Blade thickness = 20 mm Number of blades = 22	-	0.5 at TSR = 0.2	-
Kurniawati et al. [107]	2018	Experimental	Number of blades = 8, 16, and 20 Wind speed = 2 to 5 m/s	Number of blades = 16	-	0.21 at TSR = 0.59	0.38 at TSR = 0.4
Makarim et al. [108]	2018	CFD-2D	Number of blades = 16, 19, and 22 Blade depth ratio = 10%, 20%, and 30% TSR = 0, 0.109, 0.218, 0.327, and 0.436	Number of blades = 16 Blade depth ratio = 10% TSR = 0.436	-	0.187	-
Susanto et al. [112]	2018	Experimental	Number of blades = 16, 20, and 24 Rotor diameter ratio = 0.58, 0.63, 0.68, and 0.73 Wind speed = 3 to 4 m/s	Number of blades = 20 Rotor diameter ratio = 0.68	-	0.049 at TSR = 0.34	0.185 at TSR = 0.19
Tjahjana et al. [113]	2018	CFD-2D	Number of blades = 16, 20 and 24 Rotor diameter ratio = 0.58, 0.63, 0.68, and 0.73 Wind speed = 2 m/s TSR = 0.1 to 0.4	Number of blades = 20 Rotor diameter ratio = 0.68	-	0.5 at TSR = 0.3	3.1 at TSR = 0.1

Table 3. Cont.

Author	Year	Method	Turbine Design	Optimum Value (s) of Parameter	Remarks	Maximum C_p	Maximum C_T
Wibowo et al. [109]	2018	Experimental	Number of blades = 8, 12, and 16 Number of ODGV's blade = 8, 12, and 16 The tilt angle of ODGV = 20° and 60°	Number of blades = 16 Number of ODGV's blade = 16 The tilt angle of ODGV = 60°	-	0.1 at TSR = 0.28	-
Permadi and Siregar. [105]	2018	Experimental	Number of blades = 6, 8, and 12	Number of blades = 12	3.76% increase in efficiency at wind speed of 5.52 m/s	-	-
Pujol et al. [115]	2018	Experimental and CFD-2D	Number of blades = 6, 11, and 22 Use CFWT as a single rotor in VAWT or as blades in HAWT	As a single rotor in HAWT with 22 blades	-	0.41 at TSR = 0.7	-
Oktavitasari et al. [118]	2018	Numerical (CFD-2D)	Configuration = aligned and staggered Turbine distance = 0.5D, 1D, and 1.5D Wind speed = 2 m/s	Staggered 0.5D	The appropriate distance between WTs would increase by 10% of power density	-	-
Santoso et al. [122]	2018	Experimental	Angle of blade = 30°, 45°, 60°, and 90° Blade radius = 60, 90, and 120 Wind speed = 2.8 to 4.3 m/s Rotor radius ratio (Inner to outer radius ratio) = 0.73	Angle of blade = 45° Blade radius = 90	-	0.41 at TSR = 0.76	-
Larin et al. [110]	2016	CFD-3D	Number of blades = 1 to 7 30° circumferential cut on blades = without, single and double-cut In 8 different positions on the top of the building TSR = 0.6 to 0.9	7-bladed turbine with double-cut blades	-	0.24 at TSR = 0.56	-
Chiarelli et al. [120,121]	2015, 2013	Experimental and Numerical (CFD-2D)	Rotor diameter = 0.25, 1, 4, 10, and 20 m Wind speed = 10, 15, and 20 m/s	Rotor diameter = 4 m Wind speed = 10 m/s	The bigger the rotor diameter, the higher the efficiency	0.35 at TSR = 0.4	-

Table 3. Cont.

Author	Year	Method	Turbine Design	Optimum Value (s) of Parameter	Remarks	Maximum C_p	Maximum C_T
Kacor et al. [123]	2011	Numerical	Two different angles of the blade (Option A and B)	-	Options A and B have mean torque values of 3.2 Nm and 1.8 Nm, respectively	-	-
Colley et al. [106]	2009	CFD-2D	Number of blades = 3, 6, and 12 Number of stator blades = 3, 6, and 12 TSR = 0 to 0.6	Number of blades = 12 Number of stator blades = 12	Peak power output decreases due to the reduction in stator/rotor blade number	-	-
Sato et al. [117]	2005	Numerical (CFD-2D)	Install multiple CFWTs in a line Angle of attack = 0°, 30°, 60°, and 90°	Angle of attack = 0° and 30°	The turbine's performance got lowest at 90° in these calculations	-	-

5. Augmentation Devices for CFWT

The wind is variable by nature—the direction of the wind and its speed change at every moment. Despite obstacles (tall buildings and trees), these changes will be intensified in urban areas and cause turbulent and multi-directional fluid flows. Finally, turbulent flow entry into the turbine reduces its efficiency. Thus, many researchers have tried to improve its performance by designing and optimizing the devices that steer the wind flow into the turbine. The following are ways to increase the efficiency of the turbine. A summary of the augmentation devices and their advantages/disadvantages, which will be discussed in detail, is provided in Table 4.

Table 4. Summary of the augmentation devices and their advantages/disadvantages (A star means the augmentation device has this characteristic).

	Guide Nozzle	Casing	Windshield	Guide Vane	Deflector	Cowling	ODGV	Zephyr
Advantage								
Suitable for low wind speed areas	*	*						
Reduction of negative torque by preventing the wind flow from hitting the convex blades	*	*	*	*	*	*		
Converging the wind flow and increasing the input wind flow rate to the rotor	*	*						
Preventing a sudden drop in pressure behind the blades at the outlet		*						
Steering the wind flow				*	*			
Manually adjust the angle					*			
Suitable for turbulent wind flow with sudden direction changes						*		
Allowing only one-way wind to enter						*		
Having a rotating mechanism for adjustment with wind direction changes						*		
The hood enhances the pressure difference between the outlet and the turbine center and leads to increasing the turbine propulsion						*		
Suitable for multi-directional winds							*	*
No requirement for a rotating mechanism							*	*
Stator blades are designed to improve the turbine's self-starting and reduce the negative torque and rotational speed fluctuations							*	
Changing the wind flow direction to a certain angle								*
Reduction in the flow turbulence								*
Disadvantage								
Fixed position and angle	*	*	*					
Inappropriate for multi-directional winds	*	*				*		
Installation requires a surface				*				
Not automatically changing its angle				*	*			

5.1. Guide Nozzle

The converging nozzle at the inlet section of a turbine increases wind speed when it hits the blades, thereby enhancing the efficiency. Since wind angle constantly changes at WTs, this method is widely used in hydroelectric turbines. Shikha et al. [124] used a converging nozzle (Figure 13a) to concentrate wind flow and increase turbine power, which is suitable for low wind speed areas. In the wind tunnel study, they tested three parameters: the number of blades, nozzle length, and the ratio of the inlet to outlet cross-section. The best result was in the six blades, a nozzle length of 55 cm, and an input/output ratio of 0.15, which increased wind speed by 3.7 times. Figure 14 shows another study by Son et al. [125] that used two curved and straight nozzles. The CFD simulations demonstrated that the curved nozzle is more efficient than the straight nozzle and has doubled the power coefficient ($C_{P,max} = 0.265$). In addition, Krishan et al. [126] performed a 3D-CFD simulation of a CFWT with a diffuser-shaped shroud section, as shown in Figure 13b, at the top of the building. They concluded that the C_P could be improved from 0.135 to 0.34 by relocation and changing the nozzle input angle. Kang et al. [94] optimized CFWTs for an Oscillating Water Column Wave Energy Converter. According to Figure 15, the optimized model had 36 blades with 3 mm thickness and 0.38 nozzle throat width ratio. According to the authors,

the maximum efficiency of the optimized model was 0.611, which was 1.7% higher than the reference model.



Figure 13. (a) 6-blade CFWT with converging nozzle and (b) the CFWT with diffuser-shaped shroud.

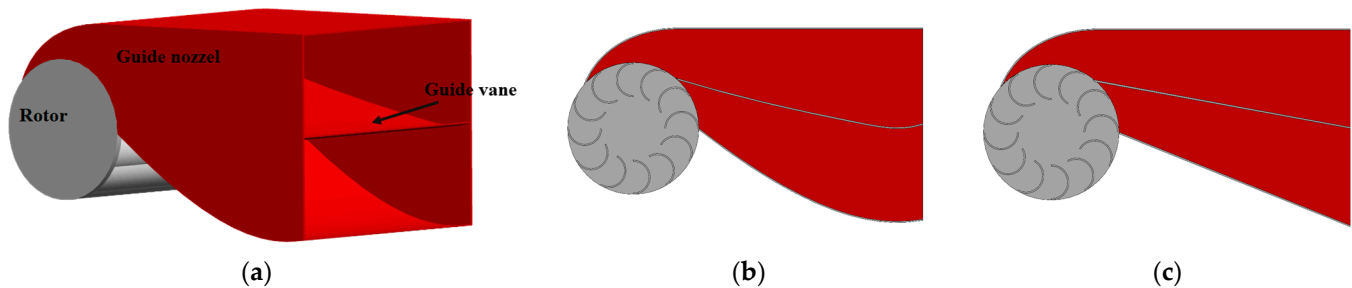


Figure 14. (a) Schematic diagram of the CFWT and guide nozzle, side view of the CFWT with (b) curved nozzle, and (c) straight nozzle.

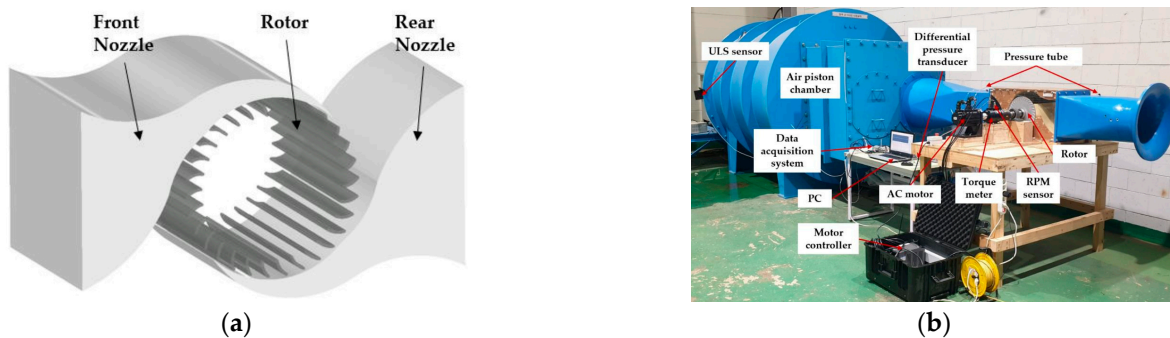


Figure 15. (a) 3D model of the CFWT with front and rear nozzles and (b) wave simulator setup [94].

5.2. Casing

A casing usually acts like a nozzle at the inlet by directing flow to the blades and a diffuser at the outlet by preventing a sudden drop in pressure behind the blades. Shigemitsu et al. [127] analyzed the two types of casing and the position of the side board (in the beginning or end of the casing). According to Figure 16a, in CFD and experimental analysis, the $C_{P,max}$ was obtained as 0.19 for casing 2, side board at the end, and a 30° inclination angle. In other studies [128,129] focusing mainly on the position of the side board (Figure 16b), they concluded that the $C_{P,max}$ was 0.17 with position 5 (P5), 72% more than the rotor without casing and side board. Likewise, by changing the casing height (Figure 16c), the $C_{P,max}$ is 0.19 with casing C2, which is 94% higher than the one without casing [130]. Also, the other two types of casing were tested; the result shows that an increase of 1.5 times of the C_p has been achieved ($C_{P,max} = 0.22$) in the presence of casing 2, compared to the state that it is absent [131].

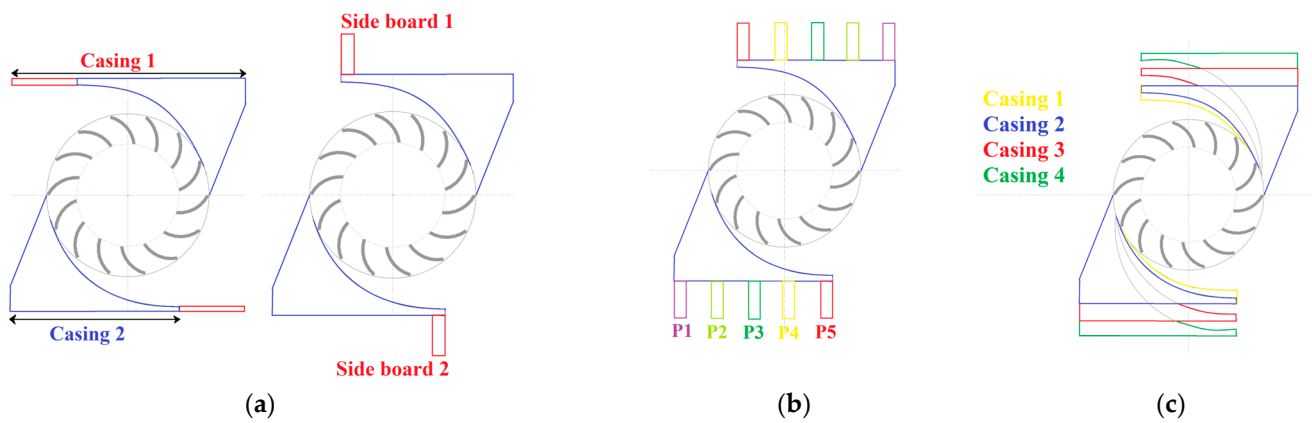


Figure 16. Side view of (a) the symmetrical casings and side boards, (b) different positions of side board, and (c) different height of casing.

5.3. Windshield

Another type of fluid flow guidance method is to use a windshield. Figure 17a shows a windshield wrapped around the turbine at a 90° angle. In this case, the C_p reaches 0.278, which increases 67% compared to the turbine without the windshield [132,133]. A CFWT simulated with a windshield at different angles along the highways shows that when a car is passing, the 60° windshield increases the captured energy by the VAWT up to 16.14% [91]. The location of a windshield is as important as its angle. This location on the upstream side (e.g., A in Figure 17b) slows the flow behind itself, which prevents the drag from acting against the rotation of the turbine. If the downstream windshield is present (e.g., B in Figure 17b), more fluid will capture into the turbine. This flow helps to rotate the turbine [99]. Also, the windshield setting angle was investigated between the values of $\Psi = 9^\circ$ and 18° , as shown in Figure 17c. The $C_{p,max}$ obtained for $\Psi = 9^\circ$ and $TSR = 0.4\sim 0.5$ is about twice as large as that for the case without the windshield [134].

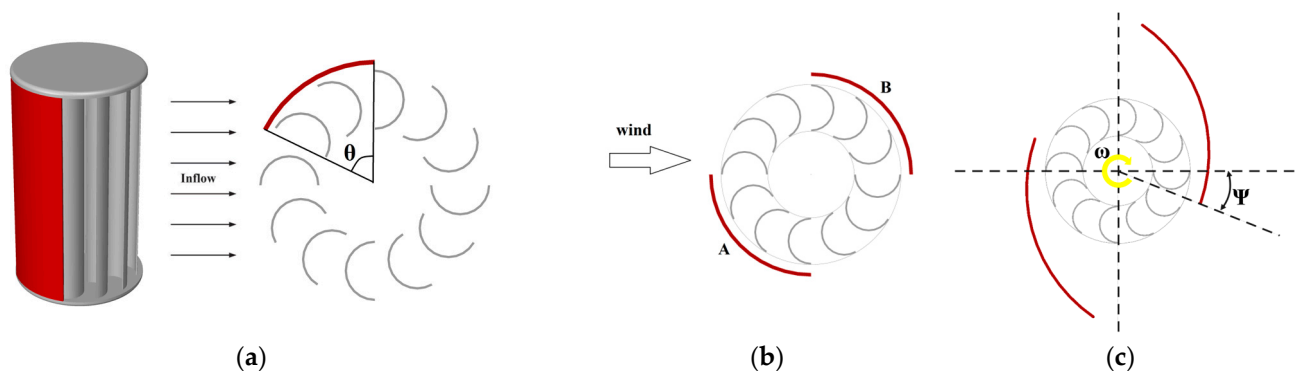


Figure 17. (a) 3D and cross-sectional view of the windshield by arc length, θ , (b) different location of windshields, and (c) improved design configuration with windshields at setting angle.

Results of experimental research [135] demonstrate that the wind concentrator (Figure 18) greatly enhances the $C_{p,max}$ of the CFWT from 0.12 (without the windshield and the wind concentrator) to 0.25 (with the windshield and the wind concentrator) by 108%. However, the arc-shaped windshield improves it by only 48% from 0.12 to 0.17 (with the windshield).

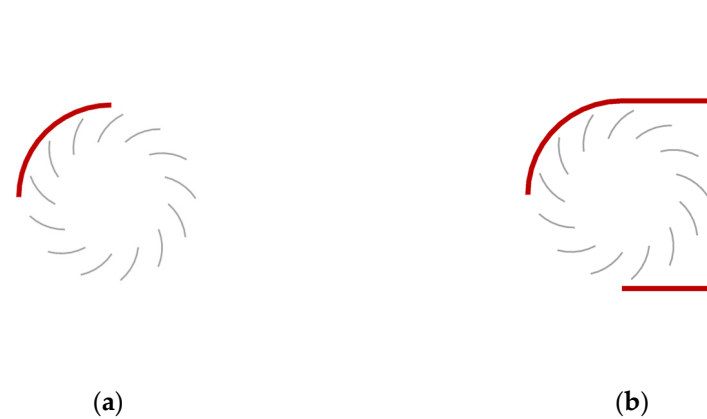


Figure 18. Cross-sectional view of (a) arc-shaped windshield and (b) wind concentrator (dimensions are [mm]).

5.4. Guide Vane

CFWT performance can also be improved by using a vane at the beginning of the turbine to steer the wind and prevent it from hitting the convex part of the rotor blades. As illustrated in Figure 19a, Tanino et al. [136] enhanced 30% of the CFWT performance by using a deflector and an Inlet Guide Vane (GV). The deflector was set near a CFWT, and an inlet GV was placed on the structure's edge, improving the wind flow inside the WT. Subsequently, the $C_{P,max}$ was 15% to 40% higher, and the TSR range showing the high C_P was wide. Furthermore, Santoso and Tjahjana [137] positioned a CFWT at the discharge outlet of a cooling tower model. They demonstrate when the GV was 150 mm from the center, and at the angle of 30° , the turbine had the highest C_P of 0.49. In short, the C_P increased by 84.3% compared to the CFWT without GV.

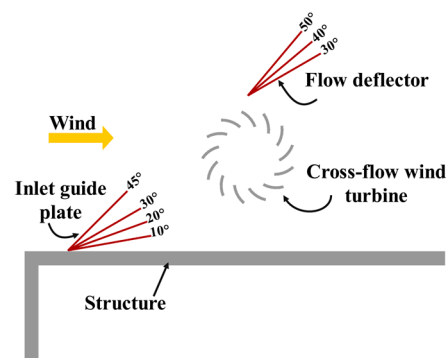


Figure 19. Side view of CFWT with GV and deflector at different angles.

5.5. Deflector

The deflectors act in similar GVs, and except the angle, can be adjusted manually after installing the turbine. In addition to investigating the effect of the GV on turbine performance, Tanino et al. [136] also tested the deflector effect. They recommended that the GV and deflector could significantly increase power production in future designs. Tian et al. [138] conducted a 2D transient CFD simulation to quantify the effects of a novel pitch-adjustable deflector they called passive-pitch shield (PPS). As shown in Figure 20, their PPS could passively adjust its pitch angle and improve the efficiency of the CFWT in all wind directions. The $C_{P,max}$ of the CFWT is increased by 46.32% with type A. Changing the deflection angle of the upstream plate can effectively increase the torque and power of the CFWT. Conversely, the arc-type upstream plate (Figure 20d) is unsuitable for improving turbine performance. A CFD model was implemented in another study [139] to train and validate the genetic algorithm combined with an artificial neural network. According to Figure 21, this method was applied to design the deflectors of an actual 8-blade, 1 kW, and

2.5 m height CFWT. Optimized deflectors increased turbine efficiency by 30%, from 0.215 to 0.279. Compared to classical simulation-based optimization, this method reduces up to 97% of the computational cost.

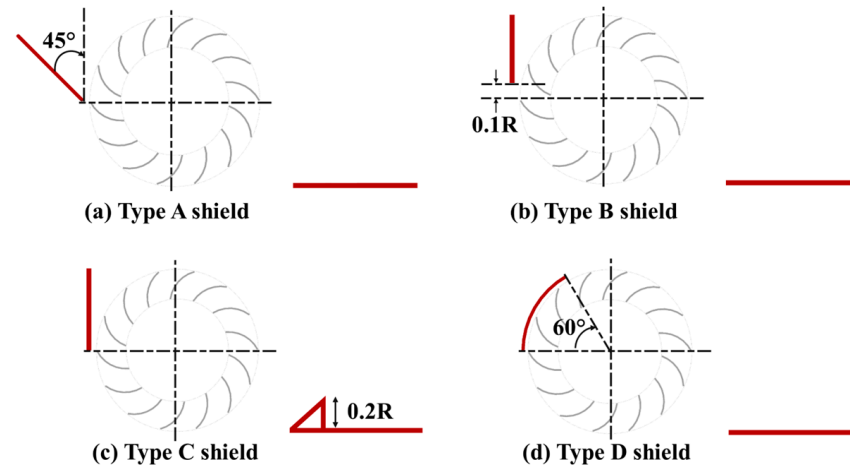


Figure 20. Schematic of four different shield and deflector designs.

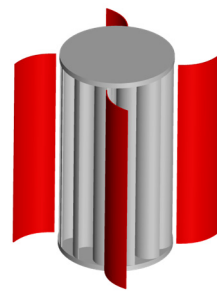


Figure 21. Schematic of the VAWT and deflector plates.

5.6. Cowling

This type of design is suitable for turbulent wind flow with sudden direction changes. According to Figure 22, the cowling around the turbine allows one-way wind to enter, i.e., half of the cylindrical shell in the inlet area is closed to prevent the wind flow from hitting the blade's convex part. When the cowling input is not in the wind direction, the canopy of the cowling plays the role of a rotating mechanism (rotator). The cowling comprises a rotary duct and a discharge tube (hood/shroud). The rotary duct is perpendicular to the center of the turbine and causes the incoming wind flow to circulate inside the turbine and exit through the hood. Moreover, the hood causes a pressure difference between the outlet and the center of the turbine, and this low-pressure rotational flow can increase the turbine propulsion. As a result, the turbine blades rotate faster [140,141].

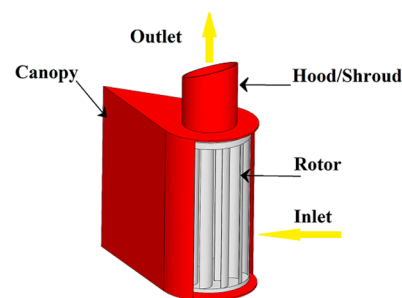


Figure 22. Schematic of CFWT with cowling.

Another prototype [142] was tested on two types of turbines with 8 and 16 blades. Respectively, 26% and 40% increases in rotor angular velocity were observed. A 3D study [143] (Figure 23) investigated mass swallowing capacities and corresponding efficiencies to the proposed casings and blade profiles at low Reynolds numbers. Another design investigation [144] was pursued by machine learning algorithms coupled with CFD, and at first, sensitivity analysis revealed the most important parameters and then determined their optimal value. Finally, with $C_{P,max}$ of 0.29 at $Re_c = 1.7 \times 10^5$, a 103% improvement over the original design was obtained.

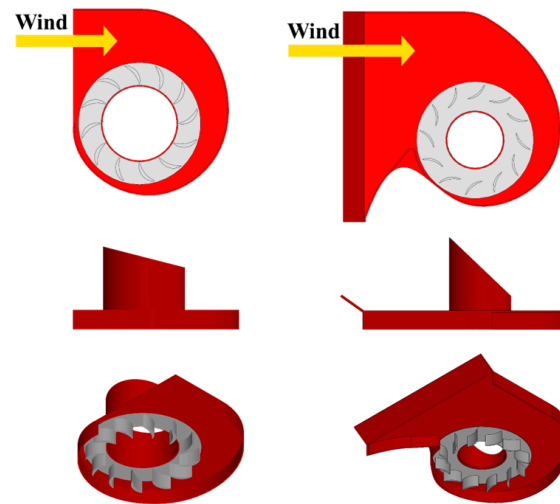


Figure 23. Comparison of the original design (left) and the optimized final design (right).

5.7. ODGV

One of the main limitations of the above devices is that they are only used for one-direction wind flow, not for multi-direction, whereas in nature, the wind blows in any direction. The rotating mechanism does not appear to be very efficient. One solution is ODGV, consisting of an upper and a lower wall with several blades or GVs. The blades are fixed and designed based on the blade angle of attack to improve the turbine self-starting and reduce the negative torque and rotational speed fluctuations. Overall, no requirement for a rotating mechanism, low cut-in speed, and increasing angular velocity are the advantages of this design. Low cut-in speed is an advantage, although it is worth investigating if this can be of practical advantage in reality. That is mainly due to the cubic dependence of the output power of the turbine on the wind speed, as well as the low efficiency of mechanical and electrical systems at partial load operations. Indeed, the impression is that even if some electrical energy is generated at 2 m/s wind speed, it should be extremely small.

In an experimental study, Wicaksono et al. [145] evaluated the effect of ODGV and concluded that the C_p increased by 21.46%. Chong et al. [146,147] performed numerical and experimental analysis for ODGV with four pairs of blades at 20° and 55° angles (Figure 24a). Their results showed a 182% increase in the blade angular velocity. According to Figure 24b, Wong et al. [148] illustrated that if these four pairs of blades bent with an angle of 10° in the middle, it reduced the cut-in speed. It improved the turbine start-up, and the C_p increased by 31.6% compared to the ODGV without a bend and 147.1% relative to the turbine without ODGV.

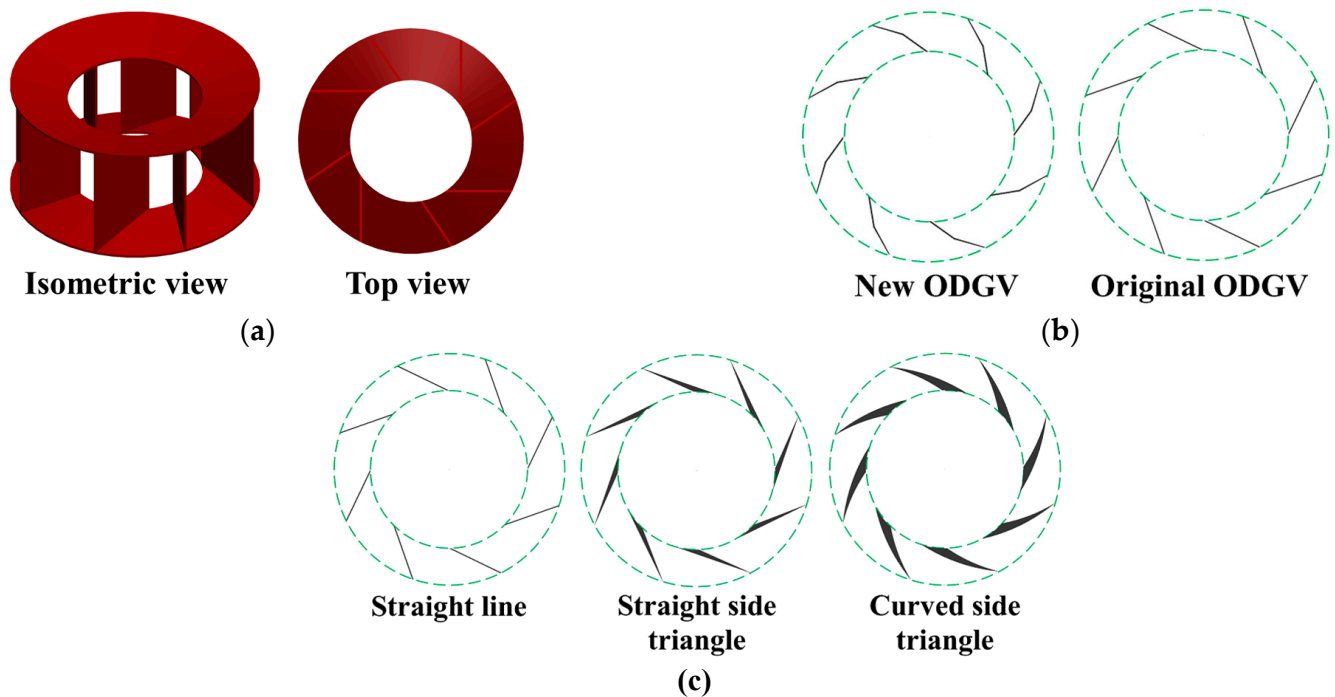


Figure 24. (a) Views and dimensions of the fabricated ODGV, (b) Design of ODGV blade with tilt angle, (c) Shapes of ODGV blade.

Subsequently, Korprasertsak et al. [149] achieved a 48% and 51.4% increase in C_p compared to turbines without ODGV, respectively, using curved and direct blades in ODGV (Figure 24c). The number and tilt angle of blades also affects the C_p and TSR. Additionally, an experiment [150] including 4, 5, and 6 blades was performed at a tilt angle of 0° , 20° , 40° , and 60° . The optimal state was 6 blades at a tilt angle of 60° . Another experiment [109] focused on the CFWT rotor as well. The optimal state of 16 CFWT blades with 16 ODGV blades was obtained at a tilt angle of 60° , with a 49% increase in C_p compared to turbines without ODGV. Similarly, Shimizu et al. [77] tested ODGV with 3, 4, 6, and 8 blades at tilt angles of 0° , 30° , and 60° with blade lengths of R and 2R (R is rotor radius). They acknowledged that with 3 blades at 2R lengths at 30° , a 120% increase in $C_{p,max}$ was achieved compared to a case without ODGV. Akabane [151] and Motohashi [152] experimentally installed 2–6 ODGV blades and demonstrated that a C_p of 0.15–0.25 could be achieved with this configuration. In summary, peak power output increases due to the increase in ODGV blade number [106].

Another similar design was proposed by Noble et al. [153], who used the eight NACA0018 airfoil types as blades and two conical surfaces. As the outer edges of the conical surfaces promote turbulent mixing above and below, the stator back pressure is reduced, and the WT power output is increased. The simulation results showed that the average C_p and C_T increased by about 30% to 35% compared to turbines without ODGV.

5.8. Zephyr

A zephyr consists of 9 blades placed around the CFWT, as illustrated in Figure 25. Due to the special shape of its blades, the zephyr reduces the flow turbulence and changes the direction of wind flow to a certain angle so that the CFWT can absorb more energy. A CFD simulation using k- ϵ turbulence model and WTE shows that the zephyr can increase the C_p from 0.098 to 0.12 [154,155].

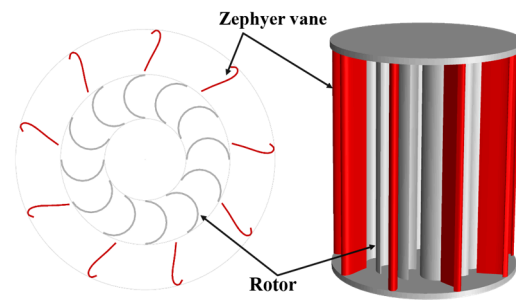


Figure 25. A zephyr prototype.

6. Wind Energy in Buildings

6.1. The Importance of a Suitable Site Location

Site location is the essential and primary factor for understanding the wind behavior, selecting WTs' type and scale, designing the wind farms (WF), and measuring their effectiveness [156]. Figure 26 shows some of the best urban and non-urban WF locations. Before starting the construction of a WF, it is necessary to perform the WRA [157,158] to estimate the potential locations and identify wind characteristics accurately. The widely used methods of WRA include measurement [159], measure-correlate-predict [160], wind atlas methodology [161], Mesoscale modelling [162], and combined Mesoscale–Microscale modelling [163]. Also, in WRA, the uncertainty in the data that affects the WT output and capital expense (CAPEX) must be considered [158,164,165]. The choice of turbine type largely depends on the site location, so for non-urban WF, large-scale HAWTs are commonly preferred [34]. However, SSWTs are the best options in urban areas due to vibration, noise, safety, visual impacts, high cut-in speed, and unpredictable efficiency change in an urban environment [166].



Figure 26. Urban and non-urban WF locations.

Main wind characteristics (e.g., speed, direction, and profile of the wind, scales and intensity of turbulence as well as surface drag) in urban areas are greatly affected by urban morphology, surface roughness, weather temperature, latitude, longitude, and elevation of the site location [167].

6.2. Environmental, Social, and Economic Aspects

Wind energy has evolved exponentially in the last few years, and its environmental, social, and economic aspects have become more apparent. Noise, vibration, light reflection, visual impacts, effects on birds, and shadows are the most critical environmental issues [168]. Nevertheless, the economic aspects are more complex than the environmental, because economic issues are multidimensional and vary between countries and regions.

For example, the Levelized Cost of Energy (LCoE) depends heavily on local conditions due to various factors (construction costs, permits, tariffs) and wind generation [169].

On the other hand, social acceptability is a major challenge for WT development, as it encompasses a wide range of stakeholders [170]. In addition, a variety of elements can affect it, such as costs, properties and results of the project, public interest and welfare, property costs, and environmental impacts in residential areas [171]. These aspects must be considered in new wind power projects to reduce project risk.

6.3. Applications in Urban Buildings

If the urban area has low-density buildings, highly open space, and is away from the grid or unstable power, stand-alone WTs—a medium-scale HAWT—are used to generate electricity [172]. One of the techniques considered in high-density urban areas is to use a small-scale VAWT, which is designed for retrofitting existing buildings [146,173]. The building height, shape, roof shape, and distance between the buildings significantly affect the wind flow; thus, it can remarkably affect the turbine type and power output. Several studies have been performed to determine the different parameters, their effectiveness, the adequate kind of turbine, and its efficiency in three scales, i.e., isolated building [110,126], [174–181], building influenced by surrounding buildings, [182–189] and real city [190–195]; see Table 5. Moreover, the CFWT, which is a small-scale turbine, can be used in buildings instead of VAWTs. Artificial Intelligence (AI) approaches can be used for the identification and assessment of wind power, WT locations, and their performance in urban environments by using the validated CFD literature in various urban configurations [196–199]. Recently, these approaches have become popular due to their high precision, strong adaptability, and improved learning capability.

In addition, WTs can be fully integrated into the building's architectural design; for example, between building blocks and inside or on the corners of the building. Figure 27 depicts three main types of urban wind energy harvesting systems.



Figure 27. Urban wind energy harvesting systems.

Table 5. Summary of the wind energy harvesting from building rooftop ((I) Isolated building scale; (II) Influence of surrounding buildings scale; (III) City scale.).

Author	Scale	Method	Software	Turbulence Modeling	Turbine Type	Important Features
Juan et al. (2021) [190]	III	On-site wind measurements—CFD	ANSYS Fluent	Realizable k- ϵ	-	-Estimation of annual mean wind speed, wind power density, and turbulence intensity in a real high-rise urban area according to the characteristics of buildings. -Validation of CFD with on-site measurements. -Investigation of installation locations of WTs on the rooftop.
Zhang et al. (2021) [174]	I	CFD	-	k- ϵ	-	Study of the effects of the rooftop WTs on the dispersion of air pollutants.
Longo et al. (2020) [182]	II	CFD	OpenFOAM ANSYS Fluent	RANS	Savonius	Evaluation of the surrounding buildings' effect on Savonius performance on the roof and accurately forecasts the energy production.
Shiraz et al. (2020) [191]	III	CFD	ANSYS	URANS	Darrieus	Evaluation of performance and efficiency of roof-mounted Darrieus in two low and high-density urban environments.
Vita et al. (2020) [183]	II	Wind tunnel measurements—CFD	ANSYS/CFX	LES	-	Investigate the effect of variations in turbulent input flow on flow patterns of the roofs of high-rise buildings in a realistic configuration.
Šarkić Glumac et al. (2018) [189]	II	Wind tunnel experiments	-	-	-	Experimental study of wind characteristics on the roof of a tall building surrounded by four buildings with the same geometry.
Wang et al. (2018) [175]	I	Lidar measurement—CFD	ANSYS Fluent	Realizable k- ϵ	-	Study the wind turbulence characteristics over a building, validation of results by wind lidar measurements, and WT positioning based on velocity and turbulence intensity.
Liu et al. (2017) [192]	III	CFD	ANSYS	RNG k- ϵ	-	Simulation of wind distribution in a full-scale urban model and comparison of results with a micro-scale local model.
Kono et al. (2016) [176]	I	CFD	FrontFlow/red	LES	SSWT	WT positioning under different wind directions and horizontal ratios (HAR = width/length) of a high-rise cuboid building.
Krishnan and Paraschivoiu (2016) [126]	I	CFD	Fluent	Realizable k- ϵ	CFWT	Study of performance enhancement of a CFWT with a diffuser-shaped shroud on building roofs.
Larin et al. (2016) [110]	I	CFD	ANSYS Fluent	URANS	Savonius and CFWT	Study of the behavior and performance of CFWT and Savonius mounted on the upstream edge of a building.

Table 5. Cont.

Author	Scale	Method	Software	Turbulence Modeling	Turbine Type	Important Features
Simoes and Estanqueiro (2016) [193]	III	Urban digitalterrain model-CFD	WindSim	k- ϵ	SSWT	Develop a new and simple methodology for urban WRA, assessing wind speed and power density on the building roof.
Toja-Silva et al. (2016) [184]	II	CFD	OpenFOAM	modified Durbin k- ϵ	HAWT and VAWT	Empirical-heuristic optimization of the roof shape, influence of the building aspect ratio and height of the surrounding buildings on wind flow characteristics. Positioning the WTs on the roof.
Yang et al. (2016) [194]	III	CFD	ANSYS	Realizable k- ϵ	Micro WT	Determining the potential mounting sites, estimating wind power characteristics considering urban topography, and validation with field measurements.
Toja-Silva et al. (2015a) [177]	I	CFD	OpenFOAM	RANS	HAWT and VAWT	Determining the adequate WT model according to the simulation of wind flow around an isolated building.
Toja-Silva et al. (2015b) [178]	I	CFD	OpenFOAM	modified Durbin k- ϵ	HAWT and VAWT	Investigation of the adequate roof shapes compatible with the mounting of different types of WT in high-rise buildings.
Toja-Silva et al. (2015c) [179]	I	CFD	OpenFOAM	modified Durbin k- ϵ	HAWT and VAWT	Studying the wind flow and determining the adequate WT for 1. An isolated building and 2. A building with an array of solar panels.
Wang et al. (2015) [185]	II	CFD	ANSYS	Standard k- ϵ	-	Investigating the Venturi effect in urban environments with convergent and divergent inlet mode buildings.
Tabrizi et al. (2014) [195]	III	CFD	ANSYS CFXWAsP	SST k- ω	HAWT	Combination of CFD and WAsP to evaluate urban WRA, investigate roof shape, wind direction, building height and shape, and turbine installation location in large-surface low-rise buildings.
Abohela et al. (2013) [186]	II	CFD	Fluent	Realizable k- ϵ	Micro WT	Identifying the effect of different roof shapes, urban configurations, and buildings' heights on energy efficiency and positioning of WTs on the roof
Kono et al. (2012) [180]	I	CFD	FrontFlow/red	LES	SSWT	Investigate wind power density and the standard deviation of wind velocity around a rectangular prism-shaped building
Xie et al. (2008) [188]	II	CFD	Fluent	LES	-	Simulation of flow and recognition of turbulence characteristics over random obstacles in urban areas.
Mertens et al. (2003) [181]	I	CFD	Fluent	k- ϵ	H-Darrieus	Study wind conditions on the roof and behavior of a roof-mounted H-Darrieus with respect to optimal energy efficiency.

7. Challenges and Future Scopes

An overview of numerical and experimental investigations has indicated that the performance of CFWTs depends on various parameters, and the results are improving and promising. Further, there are many untouched gaps for researchers to address in the future:

1. Although the effect of geometrical parameters on turbine efficiency has been investigated, there is a lack of studies on aspect ratio and twisting angle of blades.
2. As discussed earlier, adding an augmentation device is essential for increasing the C_p . However, they increase the total weight and design complexity. The appropriate type of augmentation choice depends on the analysis of the wind rose, project costs, installation method (HAWT or VAWT), and acceptable vibration, as well as noise. Studies have yet to fill this gap.
3. There is a scope to investigate new designs studied on other wind/hydro turbines [200,201] as augmentation devices in CFWTs.
4. More numerical investigations are essential to address the fatigue behavior and acoustic, dynamic, and structural analysis of system components, which could help improve the device performance and likewise reduce the noise and cost.
5. Systematic studies for the utilization of CFWTs are needed at the WF scale in rural buildings or urban high-rise buildings to see the technical feasibility of generating power from CFWTs under the influence of surrounding obstacles.

8. Conclusions

Although the eminent advantages of CFWTs, such as simple design, remarkable stability, self-starting ability, low noise, and cut-in speed, make them a golden option for building energy systems as a SSWT, they have been suffering from low efficiency. This paper reviews the optimization studies focusing on the design and the performance improvement of the CFWT, as well as building-mounted WTs for energy harvesting. The literature survey shows that many research projects attempted to enhance the CFWT efficiency by modifying its geometric characteristics or designing augmentation devices for that. The key findings of this literature review are as follows:

1. The output of the CFWT depends on the geometrical parameters, namely angle, thickness, and circumferential length of the blade, rotor diameter ratio, and the number of blades as well as stages. If the WF scale is considered, parameters such as turbine arrangement, type of installation (VAWT or HAWT), the distance between turbines, and the direction of rotation of each one become important.
2. In most studies, 12 and 16 blades were recommended, which can lead to the highest performance. Additionally, the double-stage rotor and 12° phase shift angle provide a good value of C_p and reduce the negative torque.
3. Selecting an appropriate TSR range can maximize C_p for various configurations.
4. In a linear configuration, two turbines with opposite rotation directions and at a 2.5D distance from each other reach the highest C_p (D represents the outer diameter of CFWT). In a farm configuration, four turbines located in a staggered arrangement within the distance S1:S2 of 0.5D:0.5D have the highest power density. Further, using the CFWT as a single rotor in VAWT is a better arrangement than using the CFWT as 5 blades in HAWT.
5. Augmentation devices include guide nozzle, casing, windshield, guide vane, deflector, cowling, ODGV, and zephyr. They reduce negative torque by preventing the wind flow from hitting the convex part of the blades or converging the wind flow, thereby increasing the C_p . Based on their advantages/disadvantages and previous discussions in the literature on efficiency improvement, ODGV and guide nozzle have the best effect on CFWT performance, as they have caused an increase of 147% and 152%, respectively, in C_p compared to the rotor without any augmentation device.
6. Most of the research focused on the application of CFWTs has investigated this turbine in busy highways and airport runways. Nevertheless, CFWTs can be effectively integrated with buildings and harvest reasonable power output. Although the efficiency

is not yet dramatically high, it could result in acceptable cost-effectiveness levels in areas with high annual wind capacity factors.

A gap has also been observed in studies on the effect of fatigue behavior and acoustic, dynamic, and structural analysis of system components, which may help improve the performance of such turbines. Studying other geometrical parameters (aspect ratio and twisting angle of blades), choosing an appropriate type of augmentation device based on various factors, investigating or innovating new designs as augmentation for CFWTs, and simulating at the WF scale in rural buildings or urban high-rise buildings are some of the shortcomings of the literature to be addressed by the research community in the future.

Understanding these all and considering the thorough information presented in the paper about CFWTs from different perspectives, one could say that this literature review could assist researchers and developers in selecting and optimizing system parameters for CFWT configurations.

Funding: This research received no external funding.

Institutional Review Board Statement: Not applicable.

Informed Consent Statement: Not applicable.

Data Availability Statement: Not applicable.

Conflicts of Interest: The authors declare no conflict of interest.

Nomenclature

Parameters/Variables			Abbreviations	
A	m^2	Area	CAPEX	Capital expense
C	-	Model constant-coefficient	CAWT	Cross axis wind turbine
C_p	-	Power coefficient	CFD	Computational fluid dynamics
C_T	-	Torque coefficient	CFF	Cross-flow fan
C_μ	-	Eddy-viscosity coefficient	CFHT	Cross-flow hydro turbine
D	m	Diameter	CFR	Cross-flow rotor
\vec{F}	N	External body forces	CFWT	Cross-flow wind turbine
G_k, G_b	$N/m^2 \cdot s$	Turbulence kinetic energy generation	HAWT	Horizontal axis wind turbine
H	m	Height	ODGV	Omni direction guide vane
I	-	Unit tensor	OWC	Oscillating Water Columns
k	m^2/s^2	Turbulence kinetic energy	PPS	Passive-pitch shield
M_t	-	Turbulent Mach number	SSWT	Small-scale wind turbine
P	W	Power	TSR	Tip speed ratio
p	pa	Pressure	VAWT	Vertical axis wind turbine
R	m	Radius	VGOT	Variable geometry oval trajectory
S_ϵ, S_k	$N/m^2 \cdot s$	User-defined source terms	WRA	Wind resource assessment
T	Nm	Torque	WT	Wind turbine
t	s	Time	WTE	Wind tunnel experiment
U	m/s	linear velocity	Subscripts and Superscripts	
u_i, v_i, w_i	m/s	Instantaneous velocity in tensor notation	r	Rotor
\vec{u}_r	m/s	Relative velocity	t	Turbulent
V	m/s	Wind speed	w	Wind power
x, y, z	m	Cartesian coordinates		
Y_M	$N/m^2 \cdot s$	Contribution of the fluctuating dilatation		

Greek symbol

α	deg	Angle of Attack
ε	m^2/s^3	Turbulence kinetic energy dissipation rate
λ	-	Tip speed ratio
μ	$\text{N}\cdot\text{s}/\text{m}^2$	Dynamic viscosity
ν	m^2/s	Kinematic viscosity
ρ	kg/m^3	Density
$\sigma_{\varepsilon}, \sigma_k$	-	Turbulent Prandtl number
τ	N/m^2	Stress tensor
ω	1/s	Specific dissipation rate
$\tilde{\omega}$	rad/s	Angular velocity

References

- Gupta, A.K. Efficient Wind Energy Conversion: Evolution to Modern Design. *J. Energy Resour. Technol.* **2015**, *137*, 051201. [CrossRef]
- Lazkano, I.; Nøstbakken, L.; Pelli, M. From fossil fuels to renewables: The role of electricity storage. *Eur. Econ. Rev.* **2017**, *99*, 113–129. [CrossRef]
- Sahu, B.K. Wind energy developments and policies in China: A short review. *Renew. Sustain. Energy Rev.* **2018**, *81*, 1393–1405. [CrossRef]
- Behzadi, A.; Arabkoohsar, A.; Yang, Y. Optimization and dynamic techno-economic analysis of a novel PVT-based smart building energy system. *Appl. Therm. Eng.* **2020**, *181*, 115926. [CrossRef]
- International Energy Agency; International Renewable Energy Agency; United Nations; World Bank Group; World Health Organization. *Tracking SDG7: The Energy Progress Report 2018*; World Bank: Washington, DC, USA, 2018; Available online: <https://openknowledge.worldbank.org/handle/10986/29812> (accessed on 3 July 2022).
- UNDP and WHO. *The Energy Access Situation in Developing Countries: A Review Focusing on the Least Developed Countries and Sub-Saharan Africa*; UNDP: New York, NY, USA, 2009.
- World Bank. *Household Cookstoves, Environment, Health, and Climate Change*; World Bank: Washington, DC, USA, 2011.
- World Health Organization (WHO). *Burden of Disease from Household Air Pollution for 2016 Description of Method*; World Health Organization: Geneva, Switzerland, 2018.
- Bazilian, M.; Nussbaumer, P.; Cabraal, A.; Centurelli, R.; Detchon, R.; Gielen, D.; Howells, M.; McMahon, H.; Modi, V.; O'gallachoir, B.; et al. *Measuring Energy Access: Supporting a Global Target*; Columbia University: New York, NY, USA, 2010; Available online: <https://pure.iiasa.ac.at/id/eprint/9372/> (accessed on 3 July 2022).
- Guo, S.; Liu, Q.; Sun, J.; Jin, H. A review on the utilization of hybrid renewable energy. *Renew. Sustain. Energy Rev.* **2018**, *91*, 1121–1147. [CrossRef]
- Nabat, M.H.; Zeynalian, M.; Razmi, A.R.; Arabkoohsar, A.; Soltani, M. Energy, exergy, and economic analyses of an innovative energy storage system; liquid air energy storage (LAES) combined with high-temperature thermal energy storage (HTES). *Energy Convers. Manag.* **2020**, *226*, 113486. [CrossRef]
- Behzadi, A.; Arabkoohsar, A. Comparative performance assessment of a novel cogeneration solar-driven building energy system integrating with various district heating designs. *Energy Convers. Manag.* **2020**, *220*, 113101. [CrossRef]
- Arabkoohsar, A. Combined steam based high-temperature heat and power storage with an Organic Rankine Cycle, an efficient mechanical electricity storage technology. *J. Clean. Prod.* **2020**, *247*, 119098. [CrossRef]
- Sundqvist, T.; Söderholm, P. Valuing the Environmental Impacts of Electricity Generation: A Critical Survey. *J. Energy Lit.* **2002**, *8*, 3–41.
- Heier, S. *Grid Integration of Wind Energy: Onshore and Offshore Conversion Systems*; John Wiley & Sons: Hoboken, NJ, USA, 2014.
- Ackermann, T.; Söder, L. Wind energy technology and current status: A review. *Renew. Sustain. Energy Rev.* **2000**, *4*, 315–374. [CrossRef]
- Ackermann, T. *Wind Power in Power Systems*; John Wiley & Sons: Hoboken, NJ, USA, 2012.
- Bull, S.R. Renewable energy today and tomorrow. *Proc. IEEE* **2001**, *89*, 1216–1226. [CrossRef]
- REN21. *Renewables 2022 Global Status Report*; REN21: Paris, France, 2022.
- Roy, S.; Saha, U.K. Review on the numerical investigations into the design and development of Savonius wind rotors. *Renew. Sustain. Energy Rev.* **2013**, *24*, 73–83. [CrossRef]
- Kang, C.; Liu, H.; Yang, X. Review of fluid dynamics aspects of Savonius-rotor-based vertical-axis wind rotors. *Renew. Sustain. Energy Rev.* **2014**, *33*, 499–508. [CrossRef]
- Tang, Z.P.; Yao, Y.X.; Zhou, L.; Yu, B.W. A review on the new structure of Savonius wind turbines. *Adv. Mater. Res.* **2013**, *608*, 467–478. [CrossRef]
- Fanel Dorel, S.; Adrian Mihai, G.; Nicusor, D. Review of Specific Performance Parameters of Vertical Wind Turbine Rotors Based on the SAVONIUS Type. *Energies* **2021**, *14*, 1962. [CrossRef]

24. Kumar, R.; Raahemifar, K.; Fung, A.S. A critical review of vertical axis wind turbines for urban applications. *Renew. Sustain. Energy Rev.* **2018**, *89*, 281–291. [CrossRef]
25. Mertens, S. *Wind Energy in the Built Environment: Concentrator Effects of Buildings*; Multi-Science: Essex, UK, 2006.
26. Simão Ferreira, C.; Van Kuik, G.; Van Bussel, G.; Scarano, F. Visualization by PIV of dynamic stall on a vertical axis wind turbine. *Exp. Fluids* **2009**, *46*, 97–108. [CrossRef]
27. Simic, Z.; Havelka, J.G.; Bozicevic Vrhovcak, M. Small wind turbines—A unique segment of the wind power market. *Renew. Energy* **2013**, *50*, 1027–1036. [CrossRef]
28. Khorsand, I.; Kormos, C.; MacDonald, E.G.; Crawford, C. Wind energy in the city: An interurban comparison of social acceptance of wind energy projects. *Energy Res. Soc. Sci.* **2015**, *8*, 66–77. [CrossRef]
29. Alom, N.; Saha, U.K. Evolution and progress in the development of savonius wind turbine rotor blade profiles and shapes. *J. Sol. Energy Eng.* **2019**, *141*, 30801. [CrossRef]
30. Kirke, B.K. *Evaluation of Self-Starting Vertical Axis Wind Turbines for Stand-Alone Applications*; Griffith University: Brisbane, Australia, 1998.
31. D'Ambrosio, M.; Medaglia, M. Vertical Axis Wind Turbines: History, Technology and Applications. 2010. Available online: <http://windharvest.com/wp-content/uploads/2018/02/Vertical-Axis-Wind-Turbines-History-Technology-and-Applications.pdf> (accessed on 29 November 2022).
32. Atash, F. The deterioration of urban environments in developing countries: Mitigating the air pollution crisis in Tehran, Iran. *Cities* **2007**, *24*, 399–409. [CrossRef]
33. Tjiu, W.; Marnoto, T.; Mat, S.; Ruslan, M.H.; Sopian, K. Darrieus vertical axis wind turbine for power generation I: Assessment of Darrieus VAWT configurations. *Renew. Energy* **2015**, *75*, 50–67. [CrossRef]
34. Tasneem, Z.; Al Noman, A.; Das, S.K.; Saha, D.K.; Islam, M.R.; Ali, M.F.; R Badal, M.F.; Ahamed, M.H.; Moyeen, S.I.; Alam, F. An analytical review on the evaluation of wind resource and wind turbine for urban application: Prospect and challenges. *Dev. Built Environ.* **2020**, *4*, 100033. [CrossRef]
35. Rajpar, A.H.; Ali, I.; Eladwi, A.E.; Bashir, M.B.A. Recent Development in the Design of Wind Deflectors for Vertical Axis Wind Turbine: A Review. *Energies* **2021**, *14*, 5140. [CrossRef]
36. Dewan, A.; Gautam, A.; Goyal, R. Savonius wind turbines: A review of recent advances in design and performance enhancements. *Mater. Today Proc.* **2021**, *47*, 2976–2983. [CrossRef]
37. Das Karmakar, S.; Chattopadhyay, H. A review of augmentation methods to enhance the performance of vertical axis wind turbine. *Sustain. Energy Technol. Assess.* **2022**, *53*, 102469. [CrossRef]
38. Cuevas-Carvajal, N.; Cortes-Ramirez, J.S.; Norato, J.A.; Hernandez, C.; Montoya-Vallejo, M.F. Effect of geometrical parameters on the performance of conventional Savonius VAWT: A review. *Renew. Sustain. Energy Rev.* **2022**, *161*, 112314. [CrossRef]
39. Cuesta, A.; Gomez-Gil, F.; Fraile, J.; Rodríguez, J.; Calvo, J.; Vara, J. Feasibility of a Simple Small Wind Turbine with Variable-Speed Regulation Made of Commercial Components. *Energies* **2013**, *6*, 3373–3391. [CrossRef]
40. Chong, W.-T.; Muzammil, W.K.; Wong, K.-H.; Wang, C.-T.; Gwani, M.; Chu, Y.-J.; Poh, S.-C. Cross axis wind turbine: Pushing the limit of wind turbine technology with complementary design. *Appl. Energy* **2017**, *207*, 78–95. [CrossRef]
41. Chong, W.-T.; Wong, K.-H.; Wang, C.-T.; Gwani, M.; Chu, Y.-J.; Chia, W.-C.; Poh, S.-C. Cross-Axis-Wind-Turbine: A Complementary Design to Push the Limit of Wind Turbine Technology. *Energy Procedia* **2017**, *105*, 973–979. [CrossRef]
42. Bardakjian, A.T.; Mandadakias, P.P.; Tingle, A. Efficiency comparison of horizontal axis wind turbines and bladeless turbines. *PAM Rev. Energy Sci. Technol.* **2017**, *4*, 59–75. [CrossRef]
43. Das, A.; Talapatra, P.K. Modelling and analysis of a mini vertical axis wind turbine. *Int. J. Emerg. Technol. Adv. Eng.* **2016**, *6*, 184–194.
44. Vidal, C.D. Diseño de un aerogenerador Savonius para uso doméstico, UNIVERSITAT POLITÈCNICA DE VALÈNCIA. 2019. Available online: <https://riunet.upv.es/handle/10251/131197> (accessed on 9 February 2023).
45. Marie, D.G.J. Turbine Having Its Rotating Shaft Transverse to the Flow of the Current. Google Patents US1835018A, 8 December 1931. Available online: <https://patents.google.com/patent/US1835018A/en> (accessed on 9 February 2023).
46. Wilson, R.E.; Lissaman, P.B.S. *Applied Aerodynamics of Wind Power Machines*; Oregon State University: Corvallis, OR, USA, 1974.
47. Savonius, S.J. The S-rotor and its applications. *Mech. Eng.* **1931**, *53*, 333–338.
48. Tummala, A.; Velamati, R.K.; Sinha, D.K.; Indraj, V.; Krishna, V.H. A review on small scale wind turbines. *Renew. Sustain. Energy Rev.* **2016**, *56*, 1351–1371. [CrossRef]
49. Arab Energy. Available online: <https://www.arabenergy.de/windelectricsystems.html> (accessed on 10 August 2021).
50. nr21 DESIGN STUDIO. Available online: <https://nr21.com/lws/> (accessed on 20 October 2021).
51. LWS Micro Turbine til Tag Eller Hjørne Montage 50 | Campen Auktioner A/S. Available online: <https://campenauktioner.hibid.com/lot/36479802/lws-micro-turbine-til-tag-eller-hj-rne-montage--50/?q=&ref=catalog> (accessed on 1 August 2021).
52. Gosman, A. Developments in CFD for industrial and environmental applications in wind engineering. *J. Wind Eng. Ind. Aerodyn.* **1999**, *81*, 21–39. [CrossRef]
53. Launder, B.E.; Spalding, D.B. The Numerical Computation of Turbulent Flows. *Comput. Methods Applied Mechanical Engineering* **1974**, *3*, 269–289. [CrossRef]
54. Shih, T.-H.; Liou, W.W.; Shabbir, A.; Yang, Z.; Zhu, J. A new k- ϵ eddy viscosity model for high reynolds number turbulent flows. *Comput. Fluids* **1995**, *24*, 227–238. [CrossRef]

55. Wilcox, D.C. Reassessment of the scale-determining equation for advanced turbulence models. *AIAA J.* **1988**, *26*, 1299–1310. [[CrossRef](#)]
56. Menter, F. Zonal Two Equation k- ω Turbulence Models For Aerodynamic Flows. In Proceedings of the 23rd Fluid Dynamics, Plasmadynamics, and Lasers Conference, Orlando, FL, USA, 6–9 July 1993. [[CrossRef](#)]
57. Menter, F.R. Two-equation eddy-viscosity turbulence models for engineering applications. *AIAA J.* **1994**, *32*, 1598–1605. [[CrossRef](#)]
58. Hansen, M. *Aerodynamics of Wind Turbines*; Routledge: London, UK, 2015.
59. Betz, A. Das Maximum der theoretisch möglichen Ausnutzung des Windes durch Windmotoren. *Z. Gesamte Turbinenwesen* **1920**, *26*, 307–309.
60. Adaramola, M. *Wind Turbine Technology: Principles and Design*; CRC Press: Boca Raton, FL, USA, 2014.
61. Tong, W. *Wind Power Generation and Wind Turbine Design*; WIT Press: Boston, MA, USA, 2010.
62. Thomson, J.R. Chapter 4. The Human–Machine Interface. *High Integr. Syst. Saf. Manag. Hazard. Ind.* **2015**, 55–73. [[CrossRef](#)]
63. Dalin, H. Improvements in Rotary Fans. GB291007A, 1928. Available online: <https://worldwide.espacenet.com/patent/search/family/020307248/publication/GB291007A?q=GB291007A> (accessed on 9 February 2023).
64. Anderson, E.L. Unit Heater and Ventilator. US1823579A, 1931. Available online: <https://worldwide.espacenet.com/patent/search/family/023831987/publication/US1823579A?q=US1823579A> (accessed on 9 February 2023).
65. Anderson, E.L. Line Flow Fan. US1838169A, 1933. Available online: <https://worldwide.espacenet.com/patent/search/family/023426100/publication/US1838169A?q=US1838169A> (accessed on 9 February 2023).
66. Buck, C.M. Pulverized Fuel Feeder. US1893857A, 1933. Available online: <https://worldwide.espacenet.com/patent/search/family/024000990/publication/US1893857A?q=US1893857A> (accessed on 9 February 2023).
67. Buck, C.M. Blower. US2033273A, 1936. Available online: <https://worldwide.espacenet.com/patent/search/family/027054408/publication/US2033273A?q=US2033273A> (accessed on 9 February 2023).
68. Banki, D. Water Turbine. US1436933A, 1922. Available online: <https://worldwide.espacenet.com/patent/search/family/023154518/publication/US1436933A?q=US1436933A> (accessed on 9 February 2023).
69. Ossberger, F. Free jet Turbine. DE361593 (C), 1922. Available online: <https://worldwide.espacenet.com/patent/search/family/007353041/publication/DE361593C?q=DE361593> (accessed on 9 February 2023).
70. Ossberger, F. Flow Turbine. DE615445 (C), 1935. Available online: <https://worldwide.espacenet.com/patent/search/family/007355252/publication/DE615445C?q=DE615445> (accessed on 9 February 2023).
71. Mandiș, I.C.; Robescu, D.N.; Bărglăzan, M.; Capitalization Of Wind Potential Using A Modified Banki Turbine. May 2008. Available online: https://www.scientificbulletin.upb.ro/rev_docs_arhiva/full86536.pdf (accessed on 9 February 2023).
72. Moga, I.C.; Robescu, D.L.; Robescu, D.N.; Bărglăzan, M. Adjustment of Banki hydraulic turbine in order to obtain electrical energy from wind potential,(ed) UPB Scientific Bulletin. *Ser. C* **2007**, *69*, 4.
73. Klemm, T.; Gabi, M.; Heraud, J.-N. Application of a cross flow fan as wind turbine. *J. Comput. Appl. Mech.* **2007**, *8*, 123–133.
74. Kawamura, T.; Takami, H.; Kuwahara, K. Computation of high Reynolds number flow around a circular cylinder with surface roughness. *Fluid Dyn. Res.* **1986**, *1*, 145–162. [[CrossRef](#)]
75. Tan, S. An Experimental Study of Cross Flow Wind Turbine. In Proceedings of the 75th JSME Spring Annual Meeting (in Japanese): Volume 3, Tokyo Institute of Technology, Tokyo, Japan, 31 March–3 April 1998; pp. 291–292.
76. Ushiyama, I.; Isshiki, N.; Chai, G.-Z. Design Configuration and Performance Evaluation of Cross-Flow Wind Rotors. *J. JSES* **1994**, *20*, 36–41.
77. Shimizu, Y.; Takada, M.; Sakata, J. Development of a high-performance cross-flow wind turbine (On the effects of ring-diffusers and multiple-guide vanes on the power augmentation for a cross-flow wind turbine). *Trans. Japan Soc. Mech. Eng. Part B* **1998**, *64*, 2958–2963. [[CrossRef](#)]
78. Tanino, T. Influence of Number of Blade and Blade Setting Angle on the Performance of a Cross-flow Wind Turbine. *Trans. Japan Soc. Mech. Eng. Ser. B* **2007**, *73*, 225–230. [[CrossRef](#)]
79. Motohashi, H. Performance Improvement of a Cross Flow Wind Turbine by Guide Vanes Considered Primary Wind Direction. *Trans. Japan Soc. Mech. Eng. Ser. B* **2004**, *70*, 105–110. [[CrossRef](#)]
80. Fukutomi, J. The characteristics and Internal Flow of The Cross-Flow Hydro-Turbine for micro turbine. *Turbomach* **2000**, *28*, 3.
81. Layeghmand, K.; Ghiasi Tabari, N.; Zarkesh, M. Improving efficiency of Savonius wind turbine by means of an airfoil-shaped deflector. *J. Braz. Soc. Mech. Sci. Eng.* **2020**, *42*, 528. [[CrossRef](#)]
82. Jang, H.; Paek, I.; Kim, S.; Jeong, D. Performance Prediction and Validation of a Small-Capacity Twisted Savonius Wind Turbine. *Energies* **2019**, *12*, 1721. [[CrossRef](#)]
83. Mo, Q.; Wen, J.; Liu, X.; Wang, J. The Brake System and Method of the Small Vertical Axis Wind Turbine. In *Proceedings of the 2016 5th International Conference on Civil, Architectural and Hydraulic Engineering (ICCAHE 2016)*; Atlantis Press: Paris, France, 2016; pp. 145–151.
84. Dai, S.F.; Liu, H.J.; Chu, Y.J.; Lam, H.F. Impact of corner modification on wind characteristics and wind energy potential over flat roofs of tall buildings. *Energy* **2022**, *241*, 122920. [[CrossRef](#)]
85. Peng, H.Y.; Abohela, I.; Hamza, N.; Dudek, S. Effect of roof shape on energy yield and positioning of roof mounted wind turbines. In Proceedings of the Building Simulation 2011: 12th Conference of International Building Performance Simulation Association, Sydney, Australia, 14–16 November; 16 November 2011; pp. 1203–1210.

86. Ismaeel, T.; Aljabair, S.; Abdulrazzaq, O.; Abood, Y. Energy recovery of moving vehicles' wakes in highways by vertical axis wind turbines. *FME Trans.* **2020**, *48*, 557–565. [CrossRef]
87. Ali, N.M.; Ammari, H. Design of a hybrid wind-solar street lighting system to power LED lights on highway poles. *AIMS Energy* **2022**, *10*, 177–190. [CrossRef]
88. Hu, W.; Jiaqiang, E.; Tan, Y.; Zhang, F.; Liao, G. Modified wind energy collection devices for harvesting convective wind energy from cars and trucks moving in the highway. *Energy* **2022**, *247*, 123454. [CrossRef]
89. Tian, W.; Song, B.; Mao, Z. Numerical investigation of wind turbines and turbine arrays on highways. *Renew. Energy* **2020**, *147*, 384–398. [CrossRef]
90. Tian, W.; Mao, Z.; Li, Y. Numerical Simulations of a VAWT in the Wake of a Moving Car. *Energies* **2017**, *10*, 478. [CrossRef]
91. Matias, I.J.T.; Danao, L.A.M.; Abuan, B.E. Numerical Investigation on the Effects of Varying the Arc length of a Windshield on the Performance of a Highway Installed Banki Wind Turbine. *Fluids* **2021**, *6*, 285. [CrossRef]
92. Tian, W.; Mao, Z.; An, X.; Zhang, B.; Wen, H. Numerical study of energy recovery from the wakes of moving vehicles on highways by using a vertical axis wind turbine. *Energy* **2017**, *141*, 715–728. [CrossRef]
93. Qusai, S.; Esraa, S.; Aseel, R. Polycarbonate Bladed Highway Wind Turbine: A Case Study. In *2021 12th International Renewable Engineering Conference (IREC)*; IEEE: Piscataway, NJ, USA, 2021; pp. 1–5. [CrossRef]
94. Kang, H.-G.; Lee, Y.-H.; Kim, C.-J.; Kang, H.-D. Design Optimization of a Cross-Flow Air Turbine for an Oscillating Water Column Wave Energy Converter. *Energies* **2022**, *15*, 2444. [CrossRef]
95. Takao, M.; Setoguchi, T. Air Turbines for Wave Energy Conversion. *Int. J. Rotating Mach.* **2012**, *2012*, 717398. [CrossRef]
96. Kang, H.-G.; Kim, B.-H.; Lee, Y.-H. A Performance Study of a Cross-flow Air Turbine Utilizing an Orifice for OWC WEC. *KSFJ J. Fluid Mach.* **2017**, *20*, 54–62. [CrossRef]
97. Seralathan, S.; Yaswanath Sri Sai, S.; Sai Teja, B.; Sri Viswanadh, M.; Narasimha Rao, C.; Hariram, V.; Micha Premkumar, T. Static structural analysis of cross flow vertical axis wind turbine. *Mater. Today Proc.* **2020**, *33*, 3630–3639. [CrossRef]
98. Schubel, P.J.; Crossley, R.J. Wind Turbine Blade Design. *Energies* **2012**, *5*, 3425–3449. [CrossRef]
99. Kawamura, T.; Sato, Y. Numerical simulation of the flow around across-flow wind turbine. *Res. Inst. Math. Anal.* **2002**, *1288*, 44–51. Available online: <https://www.kurims.kyoto-u.ac.jp/~kyodo/kokyuroku/contents/pdf/1288-5.pdf> (accessed on 6 February 2023).
100. Kawamura, T.; Sato, Y. Numerical Study of the Flow Around the High-torque Wind Turbine of Vertical Axis Type. In *Computational Fluid Dynamics 2002*; Springer: Berlin/Heidelberg, Germany, 2003; pp. 649–654.
101. Kono, T.; Yamagishi, A.; Kiwata, T.; Kimura, S.; Komatsu, N. Experimental and Numerical Investigation on the Flow Characteristics around a Cross-Flow Wind Turbine. *Energy Power Eng.* **2016**, *08*, 173–182. [CrossRef]
102. Sivamani, S.; Hemanth Prasanna, R.; Arun, J.; Christopher, M.; Micha Premkumar, T.; Bharath Kumar, P.; Yadav, Y.; Hariram, V. Assessing Small Cross Flow Wind Turbine for Urban Rooftop Power Generation. In *Advances in Smart Grid Technology*; Springer: Singapore, 2020; pp. 105–114. [CrossRef]
103. Al-Maaitah, A.A. The design of the Banki wind turbine and its testing in real wind conditions. *Renew. Energy* **1993**, *3*, 781–786. [CrossRef]
104. Arifin, Z.; Tjahjana, D.D.D.P.; Suyitno, S.; Juwana, W.E. Performance of Crossflow Wind Turbines in In-line Configuration and Opposite Rotation Direction. *J. Adv. Res. Fluid Mech. Therm. Sci.* **2021**, *81*, 131–139. [CrossRef]
105. Permadi, M.F.W.; Siregar, I.H. Uji eksperimental turbin angin sumbu vertikal jenis cross flow dengan variasi jumlah blade. *J. Tek. Mesin* **2018**, *6*, 15–31.
106. Colley, G.; Mishra, R.; Rao, H.V.; Woolhead, R. *Performance Evaluation of Three Cross Flow Vertical Axis Wind Turbine Configurations*; University of Huddersfield: Huddersfield, UK, 2009.
107. Kurniawati, D.M.; Tjahjana, D.D.D.P.; Santoso, B. Experimental investigation on performance of crossflow wind turbine as effect of blades number. In *Proceedings of the 3rd International Conference on Industrial, Mechanical, Electrical, and Chemical Engineering*, Surakarta, Indonesia, 13–14 September 2017; p. 030045. [CrossRef]
108. Makarim, D.A.; Tjahjana, D.D.D.P.; Cahyono, S.I.; Mazlan, S.A. Performance investigation of the crossflow water turbine by using CFD. *AIP Conf. Proc.* **2019**, *2097*, 030083. [CrossRef]
109. Wibowo, A.; Tjahjana, D.D.D.P.; Santoso, B.; Situmorang, M.R.C. Study of turbine and guide vanes integration to enhance the performance of cross flow vertical axis wind turbine. *AIP Conf. Proc.* **2018**, *1931*, 030043. [CrossRef]
110. Larin, P.; Paraschivoiu, M.; Aygun, C. CFD based synergistic analysis of wind turbines for roof mounted integration. *J. Wind Eng. Ind. Aerodyn.* **2016**, *156*, 1–13. [CrossRef]
111. Hidayat, A.; Ismail, A.I. Simulation of Wind Turbines with Variation of Number of Blades and Blades Angle on Turbine Performance. In *Proceedings of the Proceedings of the 1st International Conference on Industrial Technology*, Melbourne, Australia, 13–15 February 2019; pp. 115–118. [CrossRef]
112. Susanto, S.; Tjahjana, D.D.D.P.; Santoso, B. Experimental tests of the effect of rotor diameter ratio and blade number to the cross-flow wind turbine performance. *AIP Conf. Proc.* **2018**, *1931*, 030042. [CrossRef]
113. Tjahjana, D.D.D.P.; Purbaningrum, P.; Hadi, S.; Wicaksono, Y.A.; Adiputra, D. The study of the influence of the diameter ratio and blade number to the performance of the cross flow wind turbine by using 2D computational fluid dynamics modeling. *AIP Conf. Proc.* **2018**, *1931*, 030034. [CrossRef]

114. Wikantyo, F.; Oktavitasari, D.; Tjahjana, D.D.D.P.; Hadi, S.; Pramujati, B. The Effect of Blade Thickness and Number of Blade to Crossflow Wind Turbine Performance using 2D CFD Simulation. *Int. J. Innov. Technol. Explor. Eng.* **2019**, *8*, 17–21.
115. Pujol, T.; Massaguer, A.; Massaguer, E.; Montoro, L.; Comamala, M. Net Power Coefficient of Vertical and Horizontal Wind Turbines with Crossflow Runners. *Energies* **2018**, *11*, 110. [[CrossRef](#)]
116. Pertiwi, S.I.; Dwi Prija Tjahjana, D.D.; Cahyono, S.I. Experimental Study the Effect of Turbine Distance on Cross Flow Wind Turbine Performance in In-Line Configuration with Counter-Rotating Wind Turbine. *J. Adv. Res. Fluid Mech. Therm. Sci.* **2020**, *71*, 92–99. [[CrossRef](#)]
117. Sato, Y.; Kawamura, T. Numerical Study of The Interference Effects in Small Vertical Axis Wind Turbines. In Proceedings of the ASME International Mechanical Engineering Congress and Exposition, Orlando, FL, USA, 5–11 November 2005; Volume 42193, pp. 693–696.
118. Oktavitasari, D.; Kurniawan, P.; Tjahjana, D.D.D.P.; Mazlan, S.A. Study of the wind farm arrangements and wake characteristic using numerical simulation for crossflow wind turbine. *AIP Conf. Proc.* **2019**, *2097*, 030009. [[CrossRef](#)]
119. Fahrudin; Tjahjana, D.D.D.P.; Santoso, B. Experimental study of separator effect and shift angle on crossflow wind turbine performance. *AIP Conf. Proc.* **2018**, *1931*, 030044. [[CrossRef](#)]
120. Chiarelli, M.R.; Massai, A.; Russo, G.; Atzeni, D.; Bianco, F. A new configuration of vertical axis wind turbine for a distributed and efficient wind power generation system. *Wind Eng.* **2013**, *37*, 305–319. [[CrossRef](#)]
121. Chiarelli, M.R.; Davide, A.; Francesco, B.; Andrea, M. A new configuration of vertical axis wind turbine: An overview on efficiency and dynamic behaviour. *J. Energy Chall. Mech.* **2015**, *2*, 23–28.
122. Santoso, B.; Tjahjana, D.D.D.P.; Picaso, G.P. A cross-flow turbine turned with non-uniform flow velocity on the cooling tower. *AIP Conf. Proc.* **2019**, *2097*, 030049. [[CrossRef](#)]
123. Kacor, P.; Misak, S.; Prokop, L. Modification of construction design of vertical axis wind turbine. In *Proceedings of the Annals of DAAAM for 2011 & Proceedings of the 22nd International DAAAM Symposium*; Vienna, Austria, 3–26 November 2011, Volume 22.
124. Shikha; Bhatti, T.S.; Kothari, D.P. Vertical Axis Wind Rotor with Concentration by Convergent Nozzles. *Wind Eng.* **2003**, *27*, 555–559. [[CrossRef](#)]
125. Son, S.-W.; Singh, P.M.; Choi, Y.-D. Influence of guide vane shape on the performance and internal flow of a cross flow wind turbine. *J. Korean Soc. Mar. Eng.* **2013**, *37*, 163–169. [[CrossRef](#)]
126. Krishnan, A.; Paraschivoiu, M. 3D analysis of building mounted VAWT with diffuser shaped shroud. *Sustain. Cities Soc.* **2016**, *27*, 160–166. [[CrossRef](#)]
127. Shigemitsu, T.; Fukutomi, J.; Takeyama, Y. Study on Performance Improvement of Cross-Flow Wind Turbine with Symmetrical Casing. *J. Environ. Eng.* **2009**, *4*, 490–501. [[CrossRef](#)]
128. Shigemitsu, T.; Fukutomi, J.; Toyohara, M. Performance and flow condition of cross-flow wind turbine with a symmetrical casing having side boards. *Int. J. Fluid Mach. Syst.* **2016**, *9*, 169–174. [[CrossRef](#)]
129. Fukutomi, J.; Shigemitsu, T.; Toyohara, M. Performance and Flow Condition of Cross-Flow Wind Turbine With a Symmetrical Casing. In Proceedings of the ASME-JSME-KSME 2011 Joint Fluids Engineering Conference: Volume 1, Symposia—Parts A, B, C, and D, Hamamatsu, Japan, 24–29 July 2011; pp. 1869–1874. [[CrossRef](#)]
130. Fukutomi, J.; Shigemitsu, T.; Daito, H. Study on performance and flow condition of a cross-flow wind turbine with a symmetrical casing. *J. Fluids Eng. Trans. ASME* **2011**, *133*, 051101. [[CrossRef](#)]
131. Takeuchi, K.; Fukutomi, J.; Kodani, H.; Horiguchi, H. Study on Performance and Internal Flow of Cross-Flow Wind Turbine. In Proceedings of the ASME/JSME 2003 4th Joint Fluids Summer Engineering Conference, Honolulu, HI, USA, 6–10 July 2003; ASME: Honolulu, HI, USA, 2003; pp. 597–602. [[CrossRef](#)]
132. MAO, Z.; WEI, C.; HUANG, W.; FAN, Y. Influence of Deflector Baffle on Performance of Banki Wind Turbine. *ACTA ARMAMEN-TARII* **2014**, *35*, 1324–1328.
133. Wenlong, T.; Baowei, S.; Zhaoyong, M. A Numerical Study on the Improvement of the Performance of a Banki Wind Turbine. *Wind Eng.* **2014**, *38*, 109–116. [[CrossRef](#)]
134. Ejiri, E.; Yabe, S.; Hase, S.; Ogiwara, M. Unsteady flow analysis of the vertical axis cross-flow wind turbine. In Proceedings of the Fluids Engineering Division Summer Meeting, Miami, FL, USA, 17–20 July 2006; Volume 47500, pp. 769–775.
135. Heragy, M.; Kono, T.; Kiwata, T. Investigating the effects of wind concentrator on power performance improvement of crossflow wind turbine. *Energy Convers. Manag.* **2022**, *255*, 115326. [[CrossRef](#)]
136. Tanino, T.; Nakao, S.; Uebayashi, G. Improving ambient wind environments of a cross-flow wind turbine near a structure by using an inlet guide structure and a flow deflector. *J. Therm. Sci.* **2005**, *14*, 242–248. [[CrossRef](#)]
137. Santoso, B.; Tjahjana, D.D.D.P. The Influence of Guide Vane to the Performance of Cross-Flow Wind Turbine on Waste Energy Harvesting System. *MATEC Web Conf.* **2018**, *159*, 02014. [[CrossRef](#)]
138. Tian, W.; Mao, Z.; Ding, H. Numerical study of a passive-pitch shield for the efficiency improvement of vertical axis wind turbines. *Energy Convers. Manag.* **2019**, *183*, 732–745. [[CrossRef](#)]
139. Storti, B.A.; Dorella, J.J.; Roman, N.D.; Peralta, I.; Albanesi, A.E. Improving the efficiency of a Savonius wind turbine by designing a set of deflector plates with a metamodel-based optimization approach. *Energy* **2019**, *186*, 115814. [[CrossRef](#)]
140. Ali, A.; Golde, S.; Alam, F.; Moria, H. Experimental and Computational Study of a Micro Vertical Axis Wind Turbine. *Procedia Eng.* **2012**, *49*, 254–262. [[CrossRef](#)]
141. Alam, F.; Golde, S. An Aerodynamic Study of a Micro Scale Vertical Axis Wind Turbine. *Procedia Eng.* **2013**, *56*, 568–572. [[CrossRef](#)]

142. Loganathan, B.; Chowdhury, H.; Mustary, I.; Alam, F. An Experimental Study of a Cyclonic Vertical Axis Wind Turbine for Domestic Scale Power Generation. *Procedia Eng.* **2015**, *105*, 686–691. [CrossRef]
143. Gürbüz, M.T.; İlhan, M.; Acarer, S.; Karadeniz, Z.H. Investigation of radial turbines for wind energy harvesting. *Proc. Inst. Mech. Eng. Part A J. Power Energy* **2019**, *233*, 659–672. [CrossRef]
144. Acarer, S.; Uyulan, Ç.; Karadeniz, Z.H. Optimization of radial inflow wind turbines for urban wind energy harvesting. *Energy* **2020**, *202*, 117772. [CrossRef]
145. Wicaksono, Y.A.; Tjahjana, D.D.D.P.; Hadi, S. Influence of omni-directional guide vane on the performance of cross-flow rotor for urban wind energy. *AIP Conf. Proc.* **2018**, *1931*, 030040. [CrossRef]
146. Chong, W.T.; Fazlizan, A.; Poh, S.C.; Pan, K.C.; Hew, W.P.; Hsiao, F.B. The design, simulation and testing of an urban vertical axis wind turbine with the omni-direction-guide-vane. *Appl. Energy* **2013**, *112*, 601–609. [CrossRef]
147. Chong, W.T.; Pan, K.C.; Poh, S.C.; Fazlizan, A.; Oon, C.S.; Badarudin, A.; Nik-Ghazali, N. Performance investigation of a power augmented vertical axis wind turbine for urban high-rise application. *Renew. Energy* **2013**, *51*, 388–397. [CrossRef]
148. Wong, K.H.; Chong, W.T.; Yap, H.T.; Fazlizan, A.; Omar, W.Z.W.; Poh, S.C.; Hsiao, F.B. The Design and Flow Simulation of a Power-augmented Shroud for Urban Wind Turbine System. *Energy Procedia* **2014**, *61*, 1275–1278. [CrossRef]
149. Korprasertsak, N.; Leephakpreeda, T. Analysis and optimal design of wind boosters for Vertical Axis Wind Turbines at low wind speed. *J. Wind Eng. Ind. Aerodyn.* **2016**, *159*, 9–18. [CrossRef]
150. Yahya, W.; Ziming, K.; Juan, W.; Qurashi, M.S.; Al-Nehari, M.; Salim, E. Influence of tilt angle and the number of guide vane blades towards the Savonius rotor performance. *Energy Rep.* **2021**, *7*, 3317–3327. [CrossRef]
151. Akabane, M. On the effect of the guide-vane on the performance of cross-flow wind turbine. *Furyoku Enerugi (Wind. Energy)* **1992**, *16*, 11–15. [CrossRef]
152. Motohashi, H. Improvement of Performance of Vertical Axis Wind Turbine by 2 Guide Vanes (2nd Report, Mechanism of Power up). *24th Wind. Energy* **2002**, 207–210. Available online: https://www.jstage.jst.go.jp/article/jweasympo1979/23/0/23_0_120/_pdf (accessed on 9 February 2023).
153. Nobile, R.; Vahdati, M.; Barlow, J.F.; Mewburn-Crook, A. Unsteady flow simulation of a vertical axis augmented wind turbine: A two-dimensional study. *J. Wind Eng. Ind. Aerodyn.* **2014**, *125*, 168–179. [CrossRef]
154. Pope, K.; Dincer, I.; Naterer, G.F. Energy and exergy efficiency comparison of horizontal and vertical axis wind turbines. *Renew. Energy* **2010**, *35*, 2102–2113. [CrossRef]
155. Pope, K.; Rodrigues, V.; Doyle, R.; Tsopelas, A.; Gravelins, R.; Naterer, G.F.; Tsang, E. Effects of stator vanes on power coefficients of a zephyr vertical axis wind turbine. *Renew. Energy* **2010**, *35*, 1043–1051. [CrossRef]
156. Sunderland, K.M.; Mills, G.; Conlon, M.F. Estimating the wind resource in an urban area: A case study of micro-wind generation potential in Dublin, Ireland. *J. Wind Eng. Ind. Aerodyn.* **2013**, *118*, 44–53. [CrossRef]
157. Landberg, L.; Myllerup, L.; Rathmann, O.; Petersen, E.L.; Jørgensen, B.H.; Badger, J.; Mortensen, N.G. Wind Resource Estimation—An Overview. *Wind Energy* **2003**, *6*, 261–271. [CrossRef]
158. Murthy, K.S.R.; Rahi, O.P. A comprehensive review of wind resource assessment. *Renew. Sustain. Energy Rev.* **2017**, *72*, 1320–1342. [CrossRef]
159. Pavageau, M.; Schatzmann, M. Wind tunnel measurements of concentration fluctuations in an urban street canyon. *Atmos. Environ.* **1999**, *33*, 3961–3971. [CrossRef]
160. Hunt, K.; Nason, G.P. Wind Speed Modelling and Short-Term Prediction Using Wavelets. *Wind Eng.* **2001**, *25*, 55–61. [CrossRef]
161. Mortensen, N.G.; Landberg, L.; Troen, I.; Lundtang Petersen, E. Wind Atlas Analysis and Application Program (WASP). 1993. Available online: https://backend.orbit.dtu.dk/ws/portalfiles/portal/106061302/ris_i_666_EN_v.1_ed.2_.pdf (accessed on 9 February 2023).
162. Jafari, S.; Sommer, T.; Chokani, N.; Abhari, R.S. Wind Resource Assessment Using a Mesoscale Model: The Effect of Horizontal Resolution. In *Volume 6: Oil and Gas Applications; Concentrating Solar Power Plants; Steam Turbines; Wind Energy*; American Society of Mechanical Engineers: New York, NY, USA, 2012; pp. 987–995. [CrossRef]
163. Carvalho, D.; Rocha, A.; Santos, C.S.; Pereira, R. Wind resource modelling in complex terrain using different mesoscale–microscale coupling techniques. *Appl. Energy* **2013**, *108*, 493–504. [CrossRef]
164. Veronesi, F.; Grassi, S.; Raubal, M. Statistical learning approach for wind resource assessment. *Renew. Sustain. Energy Rev.* **2016**, *56*, 836–850. [CrossRef]
165. Tsvetkova, O.; Ouarda, T.B.M.J. A review of sensitivity analysis practices in wind resource assessment. *Energy Convers. Manag.* **2021**, *238*, 114112. [CrossRef]
166. Škvorc, P.; Kozmar, H. Wind energy harnessing on tall buildings in urban environments. *Renew. Sustain. Energy Rev.* **2021**, *152*, 111662. [CrossRef]
167. Reja, R.K.; Amin, R.; Tasneem, Z.; Ali, M.F.; Islam, M.R.; Saha, D.K.; Badal, F.R.; Ahamed, M.H.; Moyeen, S.I.; Das, S.K. A review of the evaluation of urban wind resources: Challenges and perspectives. *Energy Build.* **2022**, *257*, 111781. [CrossRef]
168. Deltenre, Q.; Runacres, M.C. *Installation of a Small Building-Mounted Wind Turbine: A Case Study from Idea to Implementation*; Battisti, L., Ed.; Springer International Publishing: Cham, Switzerland, 2019; pp. 71–88. [CrossRef]
169. Sathyajith, M. *Wind energy: Fundamentals, Resource Analysis and Economics*; Springer Science & Business Media: Berlin, Germany, 2006.

170. Horbaly, R.; Huber, S.; Ellis, G. Large-scale wind deployment, social acceptance. *Wiley Interdiscip. Rev. Energy Environ.* **2012**, *1*, 194–205. [CrossRef]
171. Scherhauer, P.; Höltinger, S.; Salak, B.; Schauppenlehner, T.; Schmidt, J. Patterns of acceptance and non-acceptance within energy landscapes: A case study on wind energy expansion in Austria. *Energy Policy* **2017**, *109*, 863–870. [CrossRef]
172. Bindner, H.; Rosas, P.A.C.; Teodorescu, R.; Blaabjerg, F. Stand-Alone Version of the 11 kW GAIA Wind Turbine. 2004. Available online: <https://www.osti.gov/etdweb/servlets/purl/20896184> (accessed on 29 November 2022).
173. Chong, W.T.; Fazlizan, A.; Poh, S.C.; Pan, K.C.; Ping, H.W. Early development of an innovative building integrated wind, solar and rain water harvester for urban high rise application. *Energy Build.* **2012**, *47*, 201–207. [CrossRef]
174. Zhang, S.; Yang, H.; Du, B.; Ge, M. Effects of a rooftop wind turbine on the dispersion of air pollutant behind a cube-shaped building. *Theor. Appl. Mech. Lett.* **2021**, *11*, 100296. [CrossRef]
175. Wang, Q.; Wang, J.; Hou, Y.; Yuan, R.; Luo, K.; Fan, J. Micrositing of roof mounting wind turbine in urban environment: CFD simulations and lidar measurements. *Renew. Energy* **2018**, *115*, 1118–1133. [CrossRef]
176. Kono, T.; Kogaki, T.; Kiwata, T. Numerical Investigation of Wind Conditions for Roof-Mounted Wind Turbines: Effects of Wind Direction and Horizontal Aspect Ratio of a High-Rise Cuboid Building. *Energies* **2016**, *9*, 907. [CrossRef]
177. Toja-Silva, F.; Peralta, C.; Lopez-Garcia, O.; Navarro, J.; Cruz, I. Roof region dependent wind potential assessment with different RANS turbulence models. *J. Wind Eng. Ind. Aerodyn.* **2015**, *142*, 258–271. [CrossRef]
178. Toja-Silva, F.; Peralta, C.; Lopez-Garcia, O.; Navarro, J.; Cruz, I. Effect of roof-mounted solar panels on the wind energy exploitation on high-rise buildings. *J. Wind Eng. Ind. Aerodyn.* **2015**, *145*, 123–138. [CrossRef]
179. Toja-Silva, F.; Peralta, C.; Lopez-Garcia, O.; Navarro, J.; Cruz, I. On Roof Geometry for Urban Wind Energy Exploitation in High-Rise Buildings. *Computation* **2015**, *3*, 299–325. [CrossRef]
180. Kono, T.; Kogaki, T. Numerical Investigation of Wind Conditions over a Rectangular Prism-Shaped Building for Mounting Small Wind Turbines. *Wind Eng.* **2012**, *36*, 111–121. [CrossRef]
181. Mertens, S.; van Kuik, G.; van Bussel, G. Performance of an H-Darrieus in the Skewed Flow on a Roof1. *J. Sol. Energy Eng.* **2003**, *125*, 433–440. [CrossRef]
182. Longo, R.; Nicastro, P.; Natalini, M.; Schito, P.; Mereu, R.; Parente, A. Impact of urban environment on Savonius wind turbine performance: A numerical perspective. *Renew. Energy* **2020**, *156*, 407–422. [CrossRef]
183. Vita, G.; Hashmi, S.A.; Salvadori, S.; Hemida, H.; Baniotopoulos, C. Role of Inflow Turbulence and Surrounding Buildings on Large Eddy Simulations of Urban Wind Energy. *Energies* **2020**, *13*, 5208. [CrossRef]
184. Toja-Silva, F.; Lopez-Garcia, O.; Peralta, C.; Navarro, J.; Cruz, I. An empirical-heuristic optimization of the building-roof geometry for urban wind energy exploitation on high-rise buildings. *Appl. Energy* **2016**, *164*, 769–794. [CrossRef]
185. Wang, B.; Cot, L.D.; Adolphe, L.; Geoffroy, S.; Morchain, J. Estimation of wind energy over roof of two perpendicular buildings. *Energy Build.* **2015**, *88*, 57–67. [CrossRef]
186. Abohela, I.; Hamza, N.; Dudek, S. Effect of roof shape, wind direction, building height and urban configuration on the energy yield and positioning of roof mounted wind turbines. *Renew. Energy* **2013**, *50*, 1106–1118. [CrossRef]
187. Abohela, I. Effect of Roof Shape, Wind Direction, Building Height and Urban Configuration on the Energy Yield and Positioning of Roof Mounted Wind Turbines, Newcastle University, 2012. Available online: <https://doi.org/10443/1686> (accessed on 29 November 2022).
188. Xie, Z.-T.; Coceal, O.; Castro, I.P. Large-Eddy Simulation of Flows over Random Urban-like Obstacles. *Boundary-Layer Meteorol.* **2008**, *129*, 1–23. [CrossRef]
189. Šarkić Glumac, A.; Hemida, H.; Höffer, R. Wind energy potential above a high-rise building influenced by neighboring buildings: An experimental investigation. *J. Wind Eng. Ind. Aerodyn.* **2018**, *175*, 32–42. [CrossRef]
190. Juan, Y.-H.; Wen, C.-Y.; Chen, W.-Y.; Yang, A.-S. Numerical assessments of wind power potential and installation arrangements in realistic highly urbanized areas. *Renew. Sustain. Energy Rev.* **2021**, *135*, 110165. [CrossRef]
191. Zabarjad Shiraz, M.; Dilimulati, A.; Paraschivoiu, M. Wind power potential assessment of roof mounted wind turbines in cities. *Sustain. Cities Soc.* **2020**, *53*, 101905. [CrossRef]
192. Liu, S.; Pan, W.; Zhang, H.; Cheng, X.; Long, Z.; Chen, Q. CFD simulations of wind distribution in an urban community with a full-scale geometrical model. *Build. Environ.* **2017**, *117*, 11–23. [CrossRef]
193. Simões, T.; Estanqueiro, A. A new methodology for urban wind resource assessment. *Renew. Energy* **2016**, *89*, 598–605. [CrossRef]
194. Yang, A.-S.; Su, Y.-M.; Wen, C.-Y.; Juan, Y.-H.; Wang, W.-S.; Cheng, C.-H. Estimation of wind power generation in dense urban area. *Appl. Energy* **2016**, *171*, 213–230. [CrossRef]
195. Tabrizi, A.B.; Whale, J.; Lyons, T.; Urmee, T. Rooftop wind monitoring campaigns for small wind turbine applications: Effect of sampling rate and averaging period. *Renew. Energy* **2015**, *77*, 320–330. [CrossRef]
196. Higgins, S.; Stathopoulos, T. Application of artificial intelligence to urban wind energy. *Build. Environ.* **2021**, *197*, 107848. [CrossRef]
197. Lipu, M.S.H.; Miah, M.S.; Hannan, M.A.; Hussain, A.; Sarker, M.R.; Ayob, A.; Saad, M.H.M.; Mahmud, M.S. Artificial Intelligence Based Hybrid Forecasting Approaches for Wind Power Generation: Progress, Challenges and Prospects. *IEEE Access* **2021**, *9*, 102460–102489. [CrossRef]
198. Kabir, I.F.S.A.; Safiullah, F.; Ng, E.Y.K.; Tam, V.W.Y. New analytical wake models based on artificial intelligence and rivalling the benchmark full-rotor CFD predictions under both uniform and ABL inflows. *Energy* **2020**, *193*, 116761. [CrossRef]

199. Sawant, M.; Thakare, S.; Rao, A.P.; Feijóo-Lorenzo, A.E.; Bokde, N.D. A Review on State-of-the-Art Reviews in Wind-Turbine- and Wind-Farm-Related Topics. *Energies* **2021**, *14*, 2041. [[CrossRef](#)]
200. Thiyagaraj, J.; Rahamathullah, I.; Bharathiraja, R.; Anbuhezhiyan, G.; Ponshanmugakumar, A. Influence of various augmentation devices on the performance characteristics of modified four bladed fixed flip type savonius hydrokinetic turbine. *Mater. Today Proc.* **2021**, *46*, 3665–3669. [[CrossRef](#)]
201. Khan, M.J.; Iqbal, M.T.; Quaiocoe, J.E. River current energy conversion systems: Progress, prospects and challenges. *Renew. Sustain. Energy Rev.* **2008**, *12*, 2177–2193. [[CrossRef](#)]

Disclaimer/Publisher's Note: The statements, opinions and data contained in all publications are solely those of the individual author(s) and contributor(s) and not of MDPI and/or the editor(s). MDPI and/or the editor(s) disclaim responsibility for any injury to people or property resulting from any ideas, methods, instructions or products referred to in the content.